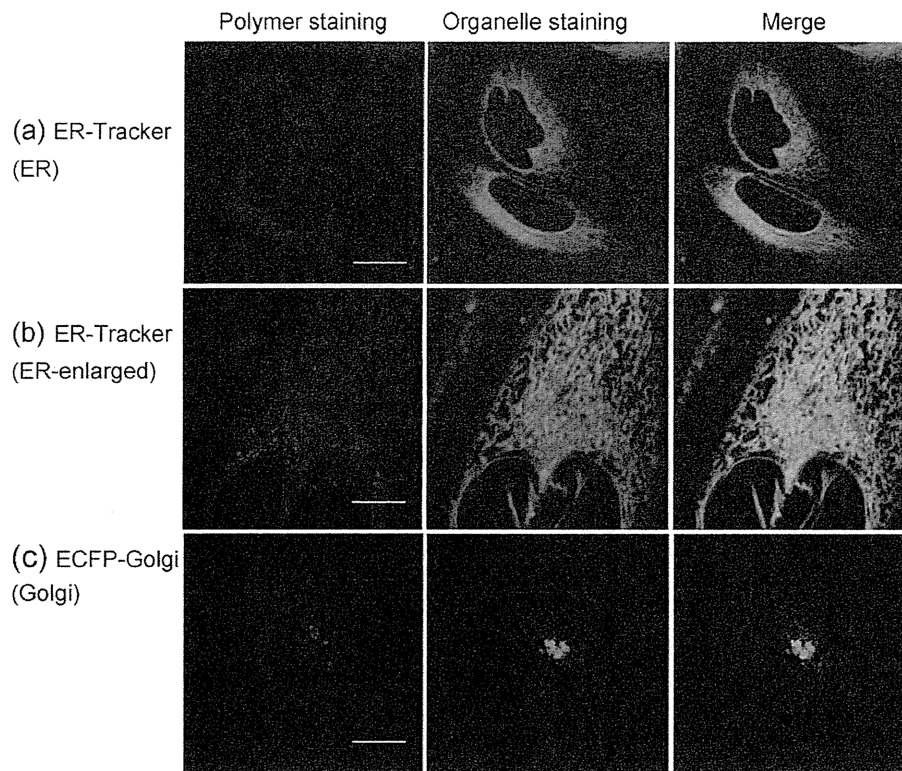

Fig. 5. Localization of Dox-bound polymers in cells co-stained with organelle-specific markers. Left, images of stained Dox-bound polymers; middle, organelle-specific fluorescent staining images; right, merged images of the left and middle images. Localization experiments using. (a and b) ER-Tracker for ER, (c) ECFP-Golgi for Golgi. Bars: 10 μm for (a) and (c). Bars: 5 μm for (b).

endosomal compartments (including lysosomes) (Richardson et al., 2008), findings consistent with our results. The perinuclear localization of the polymers is a great advantage of this system with regard to the incorporation of a nuclear-targeted drug or gene.

Most nanomaterials have been shown to exploit more than one pathway to gain cellular entry, and the pathway exploited can determine the intracellular fate (Sahay et al., 2010a). After internalization into HeLa cells, the Dox-bound polymers might be delivered to the ER directly from endosomes; in the case of cholesterol, there is some evidence for a direct pathway from endosomes to the ER (Ioannou, 2001; Mineo and Anderson, 2001). Or the polymers might be delivered to the ER directly, bypassing the endosomes/lysosomes, as do unimers of the amphiphilic triblock copolymer of poly(ethylene oxide), poly(propylene oxide), and Pluronic P85 (Sahay et al., 2010b). Simian virus 40 is known to enter the cytosol *via* the ER, suggesting that polymers distributed

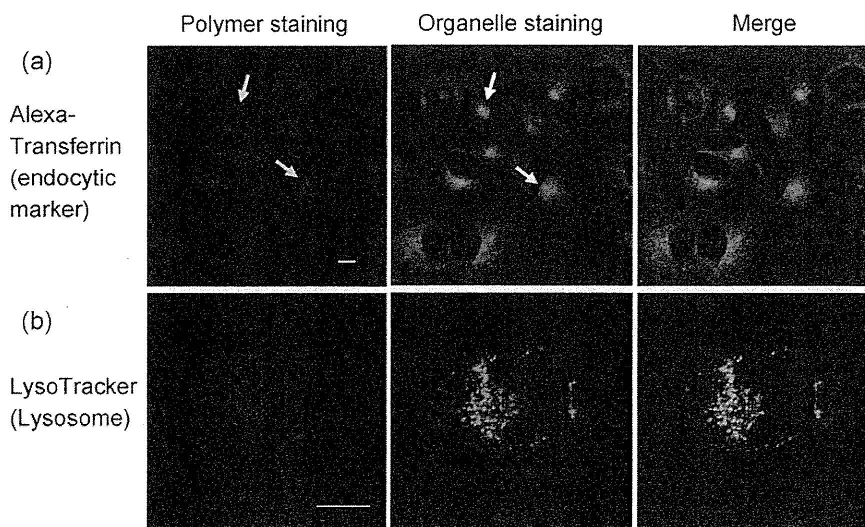

Fig. 6. Fluorescent staining images of Dox-bound polymers in cells co-stained with organelle-specific markers. Left, images of stained Dox-bound polymers; middle, organelle-specific fluorescent staining images; right, merged images of the left and middle images. Localization experiments using. (a) Alexa-transferrin, an endocytic compartment marker, and (b) LysoTracker, which is specific for lysosomes. Bars: 10 μm. Yellow and white arrows in (a) indicate the MTOC area.

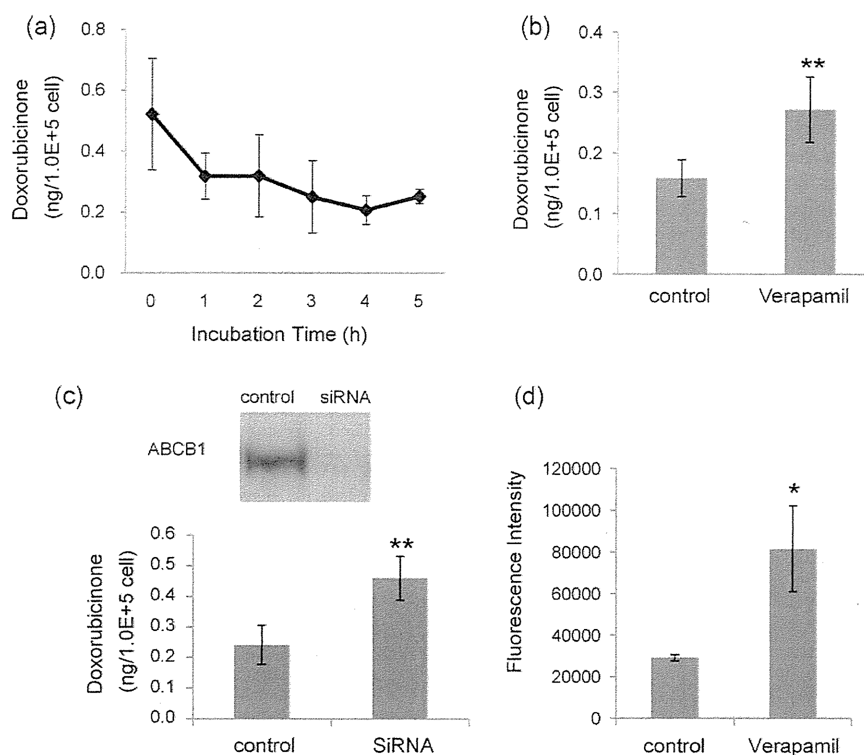

Fig. 7. Efflux of Dox-bound polymers. (a) Time-dependent change in intracellular Dox-bound polymers as indicated by released doxorubicinone. After incubation in medium with Dox-bound polymers, HeLa cells were washed and incubated with HBSS at 37 °C for the indicated durations. The doxorubicinone released by acid hydrolysis was quantitated as the amount of intracellular polymers as described in Section 2. (b) Effect of ABCB1 transporter on the efflux of Dox-bound polymers. HeLa cells were exposed to 50 μg/mL Dox-bound polymers in culture medium for 3 h. Cells were washed with 50 μg/mL verapamil or 0.1% dimethyl sulfoxide as a control. Then, the cells were incubated for another 2 h in HBSS containing the same concentration of each reagent. The amount of intracellular polymers was quantitated as the amount of doxorubicinone released by acid hydrolysis, as described in Section 2. $^{**}P < 0.01$. (c) Effect of the knockdown of ABCB1 transporter expression by siRNA on the efflux of Dox-bound polymers. Expression of ABCB1 in cell extracts was analyzed by immunoblot analysis (top). After 2 days of siRNA transfection, the cells were exposed to 50 μg/mL of Dox-bound polymers in culture medium for 3 h. After incubation, the cells were washed with HBSS and then incubated for another 2 h in HBSS without polymer. The amount of intracellular polymers was quantitated as the amount of doxorubicinone released by acid hydrolysis, as described in Section 2 (bottom). $^{**}P < 0.01$. Effect of ABCB1 transporter on the efflux of DBD-labeled polymers. HeLa cells were exposed to 50 μg/mL DBD-labeled polymers in culture medium for 24 h. Cells were washed with 50 μg/mL verapamil or 0.1% dimethyl sulfoxide as a control. Then, the cells were incubated for another 2 h in HBSS containing the same concentration of each reagent. The fluorescence intensity in a single cell was calculated as described in Section 2. $^{*}P < 0.05$.

in the ER might similarly gain access to the cytosol (Damm et al., 2005). The characteristic distribution pattern of the polymers did not change much with increasing incubation times from 0.5 to 24 h (data not shown). Although it is not clear whether the polymers maintain their structure as globular micelles or exist as unimers after internalization into a cell, increasing the dosed polymer concentration to 1 mg/mL did not change the staining pattern (data not shown). Recently, we showed PEG and poly(glutamic acid) block copolymer micelles incorporating dichloro(1,2-diaminocyclohexane)platinum(II) selectively dissociate within late endosomes (Murakami et al., 2011), suggesting that the Dox-bound polymers might also dissociate.

3.5. *Efflux of Dox-bound polymers from HeLa cells to medium*

As described in Section 3.2, the amount of intracellular Dox-bound polymers increased with time when cells were continuously exposed to Dox-bound polymers (Fig. 3a). In contrast, the amount of Dox-bound polymers gradually decreased after the Dox-bound polymers were removed from the medium (Fig. 7a). Interestingly, this decrease in the intracellular amount of Dox-bound polymers was abolished in the presence of verapamil, an inhibitor of ABCB1 (ATP-binding cassette protein B1) transporter (Fig. 7b). The ABCB1 transporter, which is also known as multidrug resistance 1 (MDR-1) or P-glycoprotein, is a member of the ABC-type transporter family and an efflux pump for various drugs. To further investigate the role of this transporter in the efflux of Dox-bound polymers from cells to medium, small interference RNAs (siRNAs) were used to target ABCB1 RNA in HeLa cells. Two days after transfection of synthetic siRNA, Western blot analysis showed that levels of ABCB1 protein expression in siRNA-transfected HeLa cells were drastically decreased (Fig. 7c), and the efflux of Dox-bound polymers from these cells was also significantly inhibited (Fig. 7c). The efflux of DBD-labeled polymers was also inhibited by ABCB1 transporter inhibitor, when intracellular fluorescent intensity of DBD-labeled polymers was measured (Fig. 7d). These results suggest that ABCB1 transporter is a key regulator of the clearance of Dox-bound polymers from HeLa cells.

It is reported that drug-binding site of ABCB1 transporter is located at a drug binding pocket that is formed by transmembrane segments and allow access of molecules directly from the membranes (Aller et al., 2009; Loo et al., 2003a,b). Furthermore, it is also known that subdomains of the ER form close contact with plasma membrane and some proteins may regulate the formation of direct membrane contacts that facilitate sterol exchange between the ER and plasma membrane (Ikonen, 2008).

Therefore, it is probable that a part of Dox-bound polymers localized in ER are transported to plasma membrane and then recognized at the drug binding site in the transmembrane segments of ABCB1 transporter.

In general, the ABCB1 transporter has very broad substrate specificity: recent studies have shown that it mediates the efflux

of a relatively large peptide, amyloid β peptide (molecular weight, 4.5 kDa), across the blood–brain barrier into the bloodstream (Cirrito et al., 2005; Kuhnke et al., 2007; Lam et al., 2001). To the best of our knowledge, the ABCB1 transporter has not been reported before to be involved in the clearance of block copolymers from cells. Because ABCB1 transporter is expressed primarily in certain normal cell types in the liver, kidney, and jejunum (Thiebaut et al., 1987), the role of ABCB1 transporter as excretion pump of Dox-bound polymer and the effect of ABCB1 transporter on the polymer blood level are probably significant from a safety perspective.

Taken together, the findings presented here suggest that Dox-bound polymers are incorporated by endocytosis. Some of the incorporated polymers are transferred to the endosome/lysosome system, and the rest may bypass the endosomal system. Then, the polymers are likely delivered to other compartments, including ER and the plasma membrane. The excretion of excess polymers from the cells is mediated by the ABCB1 transporter. Although in this system, the conjugated Dox was not designed to be released from the polymers, our results concerning intracellular trafficking and clearance of polymers would be very useful to design the carrier system where bound drugs are released from the carrier for pharmacological activity.

4. Conclusion

We investigated the intracellular trafficking of Dox-bound polymers. The polymers are internalized into cells by endocytosis, then transported to endosomal/lysosomal compartments, followed by partial distribution to the ER, or transported directly to the ER. The active excretion of the polymers from the cells may be mediated by the ABCB1 transporter. It is surprising that cells utilize their endogenous transport system for intracellular trafficking of this artificial drug carrier. Our results potentially can contribute not only to the discussion of safety issues of polymeric therapeutics but also the development of a DDS strategy utilizing or targeting this endogenous pathway more effectively.

Acknowledgements

The authors are grateful for support from Research on Publicly Essential Drugs and Medical Devices (Japan Health Sciences Foundation), a Health Labor Sciences Research Grant, and the Global COE Program for the Center for Medical System Innovation, MEXT, KAKENHI (21790046), and Nippon Kayaku Co. Ltd. We thank Mr. R. Nakamura (Nikon Corp.) for technical assistance.

References

Allen, C., Maysinger, D., Eisenberg, A., 1999. Nano-engineering block copolymer aggregates for drug delivery. Colloids Surf. B: Biointerfaces 16, 3–27.

Aller, S.G., Yu, J., Ward, A., Weng, Y., Chittaboina, S., Zhuo, R., Harrell, P.M., Trinh, Y.T., Zhang, Q., Urbatsch, I.L., Chang, G., 2009. Structure of P-glycoprotein reveals a molecular basis for poly-specific drug binding. Science 323, 1718–1722.

Bae, Y., Kataoka, K., 2009. Intelligent polymeric micelles from functional poly (ethylene glycol)-poly (amino acid) block copolymers. Adv. Drug Deliv. Rev. 61, 768–784.

Beyer, U., Rothern-Rutishauser, B., Unger, C., Wunderli-Allenspach, H., Kratz, F., 2001. Differences in the intracellular distribution of acid-sensitive doxorubicin-protein conjugates in comparison to free and liposomal formulated doxorubicin as shown by confocal microscopy. Pharm. Res. 18, 29–38.

Cirrito, J.R., Deane, R., Fagan, A.M., Spinner, M.L., Parsadanian, M., Finn, M.B., Jiang, H., Prior, J.L., Sagare, A., Bales, K.R., Paul, S.M., Zlokovic, B.V., Piwnica-Worms, D., Holtzman, D.M., 2005. P-glycoprotein deficiency at the blood-brain barrier increases amyloid-beta deposition in an Alzheimer disease mouse model. J Clin. Invest. 115, 3285–3290.

Damm, E.M., Pelkmans, L., Kartenbeck, J., Mezzacasa, A., Kurzchalia, T., Helenius, A., 2005. Clathrin- and caveolin-1-independent endocytosis: entry of simian virus 40 into cells devoid of caveolae. J. Cell Biol. 168, 477–488.

Davis, B.M., Humeau, L., Slepushkin, V., Binder, G., Korshalla, L., Ni, Y., Ogunjimi, E.O., Chang, L.F., Lu, X., Dropulic, B., 2004. ABC transporter inhibitors that are substrates enhance lentiviral vector transduction into primitive hematopoietic progenitor cells. Blood 104, 364–373.

Ferrari, M., 2005. Cancer nanotechnology: opportunities and challenges. Nat. Rev. Cancer 5, 161–171.

Hamaguchi, T., Kato, K., Yasui, H., Morizane, C., Ikeda, M., Ueno, H., Muro, K., Yamada, Y., Okusaka, T., Shirao, K., Shimada, Y., Nakahama, H., Matsumura, Y., 2007. A phase I and pharmacokinetic study of NK105, a paclitaxel-incorporating micellar nanoparticle formulation. Br. J. Cancer 97, 170–176.

Hopkins, A.L., Groom, C.R., 2002. The druggable genome. Nat. Rev. Drug Discov. 1, 727–730.

Hughes, B., 2009. Gearing up for follow-on biologics. Nat. Rev. Drug Discov. 8, 181.

Ikonen, E., 2008. Cellular cholesterol trafficking and compartmentalization. Nat. Rev. Mol. Cell Biol. 9, 125–138.

Illum, L., Davis, S.S., Müller, R.H., Mak, E., West, P., 1987. The organ distribution and circulation time of intravenously injected colloidal carriers sterically stabilized with a blockcopolymer-poloxamine 908. Life Sci. 40, 367–374.

Ioannou, Y.A., 2001. Multidrug permeases and subcellular cholesterol transport. Nat. Rev. Mol. Cell Biol. 2, 657–668.

Kataoka, K., Kwon, G.S., Yokoyama, M., Okano, T., Sakurai, Y., 1993. Block copolymer micelles as vehicles for drug delivery. J. Control. Rel. 24, 119–132.

Kataoka, K., Harada, A., Nagasaki, Y., 2001. Block copolymer micelles for drug delivery: design, characterization and biological significance. Adv. Drug Deliv. Rev. 47, 113–131.

Kolwankar, D., Glover, D.D., Ware, J.A., Tracy, T.S., 2005. Expression and function of ABCB1 and ABCG2 in human placental tissue. Drug Metab. Dispos. 33, 524–529.

Kuhnke, D., Jedlitschky, G., Grube, M., Krohn, M., Jucker, M., Mosyagin, I., Cascorbi, I., Walker, L.C., Kroemer, H.K., Warzok, R.W., Vogelgesang, S., 2007. MDR1-P-glycoprotein (ABCB1) mediates transport of Alzheimer's amyloid-β peptides – implications for the mechanisms of Aβ clearance at the blood–brain barrier. Brain Pathol. 17, 347–353.

Kuroda, J., Kuratsu, J., Yasunaga, M., Koga, Y., Saito, Y., Matsumura, Y., 2009. Potent antitumor effect of SN-38-incorporating polymeric micelle, NK012, against malignant glioma. Int. J. Cancer 124, 2505–2511.

Lam, F.C., Liu, R., Lu, P., Shapiro, A.B., Renoir, J.-M., Sharom, F.J., Reiner, P.B., 2001. β-Amyloid efflux mediated by p-glycoprotein. J. Neurochem. 76, 1121–1128.

Lavasanifar, A., Samuel, J., Kwon, G.S., 2002. Poly(ethylene oxide)-block-poly (L-amino acid) micelles for drug delivery. Adv. Drug Deliv. Rev. 54, 169–190.

Lee, S.M., Kim, J.S., 2005. Intracellular trafficking of transferrin-conjugated liposome/DNA complexes by confocal microscopy. Arch. Pharm. Res. 28, 93–99.

Lipinski, C.A., Lombardo, F., Dominy, B.W., Feeney, P.J., 2001. Experimental and computational approaches to estimate solubility and permeability in drug discovery and development settings. Adv. Drug Deliv. Rev. 46, 3–26.

Loo, T.W., Bartlett, M.C., Clarke, D.M., 2003a. Substrate-induced conformational changes in the transmembrane segments of human P-glycoprotein. J. Biol. Chem. 278, 13603–13606.

Loo, T.W., Bartlett, M.C., Clarke, D.M., 2003b. Methanethiosulfonate derivatives of rhodamine and verapamil activate human P-glycoprotein at different sites. J. Biol. Chem. 278, 50136–50141.

Manunta, M., Izzo, L., Duncan, R., Jones, A.T., 2007. Establishment of subcellular fractionation techniques to monitor the intracellular fate of polymer therapeutics. II. Identification of endosomal and lysosomal compartments in HepG2 cells combining single-step subcellular fractionation with fluorescent imaging. J. Drug Target. 15, 37–50.

Matsumura, Y., Maeda, H., 1986. A new concept for macromolecular therapeutics in cancer chemotherapy: mechanism of tumoritropic accumulation of proteins and the antitumor agent smancs. Cancer Res. 46, 6387–6392.

Matsumura, Y., Hamaguchi, T., Ura, T., Muro, K., Yamada, Y., Shimada, Y., Shirao, K., Okusaka, T., Ueno, H., Ikeda, M., Watanabe, N., 2004. Phase I clinical trial and pharmacokinetic evaluation of NK911, a micelle-encapsulated doxorubicin. Br. J. Cancer 91, 1775–1781.

Matteoni, R., Kreis, T.E., 1987. Translocation and clustering of endosomes and lysosomes depends on microtubules. J. Cell Biol. 105, 1253–1265.

Mineo, C., Anderson, R.G., 2001. Potocytosis. Robert Feulgen lecture. Histochem. Cell Biol. 116, 109–118.

Murakami, M., Cabral, H., Matsumoto, Y., Wu, S., Kano, M.R., Yamori, T., Nishiyama, N., Kataoka, K., 2011. Improving drug potency and efficacy by nanocarrier-mediated subcellular targeting. Sci. Transl. Med. 3, 64ra2.

Nakanishi, T., Fukushima, S., Okamoto, K., Suzuki, M., Matsumura, Y., Yokoyama, M., Okano, T., Sakurai, Y., Kataoka, K., 2001. Development of the polymer micelle carrier system for doxorubicin. J. Control. Rel. 74, 295–302.

Nishiyama, N., Kataoka, K., 2006. Current state, achievements, and future prospects of polymeric micelles as nanocarriers for drug and gene delivery. Pharmacol. Ther. 112, 630–648.

O'Brien, M.E.R., Wigler, N., Inbar, M., Rosso, R., Grischke, E., Santoro, A., Catane, R., Kieback, D.G., Tomczak, P., Ackland, S.P., Orlandi, F., Mellars, L., Alland, L., Tendler, C., 2004. Reduced cardiotoxicity and comparable efficacy in a phase III trial of pegylated liposomal doxorubicin HCl (CAELYX™/Doxil®) versus conventional doxorubicin for first-line treatment of metastatic breast cancer. Ann. Oncol. 15, 440–449.

Olson, R.D., Mushlin, P.S., Brenner, D.E., Fleischer, S., Cusack, B.J., Chang, B.K., Boucek Jr., R.J., 1988. Doxorubicin cardiotoxicity may be caused by its metabolite, doxorubicinol. Proc. Natl. Acad. Sci. U.S.A. 85, 3585–3589.

Rejman, J., Bragonzi, A., Conese, M., 2005. Role of clathrin- and caveolae-mediated endocytosis in gene transfer mediated by lipo- and polyplexes. Mol. Ther. 12, 468–474.
Richardson, S.C., Wallom, K.L., Ferguson, E.L., Deacon, S.P., Davies, M.W., Powell, A.J., Piper, R.C., Duncan, R., 2008. The use of fluorescence microscopy to define polymer localisation to the late endocytic compartments in cells that are targets for drug delivery. J. Control. Rel. 127, 1–11.
Sahay, G., Batrakova, E.V., Kabanov, A.V., 2008. Different internalization pathways of polymeric micelles and unimers and their effects on vesicular transport. Bioconjug. Chem. 19, 2023–2029.
Sahay, G., Alakhova, D.Y., Kabanov, A.V., 2010a. Endocytosis of nanomedicines. J. Control. Rel. 145, 182–195.
Sahay, G., Gautam, V., Luxenhofer, R., Kabanov, A.V., 2010b. The utilization of pathogen-like cellular trafficking by single chain block copolymer. Biomaterials 31, 1757–1764.
Sakai-Kato, K., Saito, E., Ishikura, K., Kawanishi, T., 2010. Analysis of intracellular doxorubicin and its metabolites by ultra-high-performance liquid chromatography. J. Chromatogr. B 878, 1466–1470.
Savić, R., Luo, L., Eisenberg, A., Maysinger, D., 2003. Micellar nanocontainers distribute to defined cytoplasmic organelles. Science 300, 615–618.
Thiebaut, F., Tsuruo, T., Hamada, H., Gottesman, M.M., Pastan, I., Willingham, M.C., 1987. Cellular localization of the multidrug-resistance gene product P-glycoprotein in normal human tissues. Proc. Natl. Acad. Sci. U.S.A. 84, 7735–7738.
Torchilin, V.P., 2002. PEG-based micelles as carriers of contrast agents for different imaging modalities. Adv. Drug Deliv. Rev. 54, 235–252.
Torchilin, V.P., Lukyanov, A.N., Gao, Z., Papahadjopoulos-Sternberg, B., 2003. Immunomicelles: targeted pharmaceutical carriers for poorly soluble drugs. Proc. Natl. Acad. Sci. U.S.A. 100, 6039–6044.
Yokoyama, M., Okano, T., Sakurai, Y., Fukushima, S., Okamoto, K., Kataoka, K., 1999. Selective delivery of adriamycin to a solid tumor using a polymeric micelle carrier system. J. Drug Target. 7, 171–186.

A New Approach to Characterization of Insulin Derived from Different Species Using ^{1}H-NMR Coupled with Multivariate Analysis

Akiko Ohno,*[,a] Toru Kawanishi,[b] Haruhiro Okuda,[a] and Kiyoshi Fukuhara[a]

[a] *Division of Organic Chemistry, National Institute of Health Sciences: and* [b] *Division of Drugs, National Institute of Health Sciences; Setagaya-ku, Tokyo 158–8501, Japan.*
Received October 7, 2011; accepted December 8, 2011; published online December 27, 2011

Most of the active components of polypeptides have a complex molecular structure, large molecular size. Such components may also be structurally heterogeneous. Therefore, development of a method that can confirm the consistency of polypeptides amino-acid sequences for product characterization is desirable. In general, it is extremely difficult to distinguish differences of a few amino acid residues in the ^{1}H-NMR spectrum of polypeptides with molecular weights greater than several thousand. However, we have been able to distinguish between three insulin species differing in one to three amino acid residues using a combination of multivariate statistics and ^{1}H-NMR spectra. These results demonstrate that this methodology could be useful for characterization of polypeptides.

Key words insulin; polypeptide; characterization; principal component analysis; ^{1}H-NMR

Nuclear magnetic resonance (NMR), which is frequently used for structure identification of unknown chemical substances in the fields of organic and natural products chemistry, is the only technique that can provide structural information on all of the components of a chemical substances. Although NMR techniques uniquely provide spectral information on primary and higher-order structure of large polymeric compounds such as polypeptides, such spectra are generally difficult to analyze in detail because of their complexity. NMR measurement has usually been applied to the structural analysis of single chemical substances, and to date, been not suitable for analyzing samples that contain multiple compounds because of the problem of overlapping peaks in the ^{1}H-NMR spectrum. However, NMR techniques have come to be used recently to analyze biogenic substances, which have made it possible to discriminate between small spectral differences by performing statistical analysis of the ^{1}H-NMR spectral data. Multivariate statistical methods, such as principal component analysis (PCA) and partial least-squares discriminate analysis (PLS-DA), are often useful for profiling and classifying sample groups and for characterizing the most effective variables of separated compounds.[1,2] Currently, multivariate statistical methods, which combine various analytical methods, have been widely used to evaluate the quality of drugs and foods, quantitatively or qualitatively, in addition to enabling predictions of drug metabolism, and toxicity.[3—10]

Compared with small-molecule drugs, polypeptides are heterogeneous and are more complex in their makeup for a number of possible reasons including mutations in the amino acid sequence of the protein, different posttranslational modifications, or by being a mixture of molecules with different terminal structures due to degradation by contaminating proteases.[11] The structural heterogeneity caused by these factors may affect the physiological activity and pharmacokinetics of polypeptides, resulting in changes in drug efficacy and safety.[11] Therefore, the development of analytical procedures that can confirm the constancy of multiple amino-acid sequences of a polypeptide for product characterization is desirable. However, characterizing the full complexity of polypeptides by presently available analytical methods is still difficult. Therefore, it is necessary to provide a more detailed evaluation of special characteristics of polypeptides by a new physicochemical index or new analytical techniques. In our recent study, it was reported that peak changes in the determination of characteristic spectral changes associated with time-dependent alterations of oxytocin (OXT) were also observed in the PCA loading plot.[8,12] Thus, the possibility of evaluating slight differences in the quality of a polypeptide was demonstrated.

In this study, we examined multivariate statistics coupled with ^{1}H-NMR to analyze the difference of amino acid sequences in three species of insulin and to show this method to be effective for the characterization of the polypeptides. As a result, we have succeeded in precisely characterizing human, bovine, and porcine insulins with sequence differences of one or three amino acids, by performing ^{1}H-NMR measurements of the individual insulins and their mixtures followed by PCA of the spectra. The results suggest that this methodology could be useful for the characterization of species-related sequence differences in polypeptides.

Experimental

Chemicals and Reagents All reagents used for ^{1}H-NMR experiments were of analytical grade (purity >99%) from Wako Chemicals and were used without further purification. Human recombinant insulin expressed in yeast (CAS# 11061-68-0) and insulin from bovine pancreas (CAS# 11070-73-8) were purchased from Aldrich (St. Louis, MO, U.S.A.); porcine insulin (CAS# 12584-58-6) was purchased from MP Biomedicals. Acetonitrile-d_3 for NMR was purchased from Acros Organics (CN). Deuterium oxide (D_2O, isotopic purity 99.9%) and 3-(trimethylsilyl) propionic-2,2,3,3-d_4 acid, sodium salt (TSP) were purchased from Aldrich (St. Louis, MO, U.S.A.). TSP was used as an internal standard with a chemical shift (δ) of 0.0 ppm in ^{1}H-NMR measurements.

Sample Preparation and ^{1}H-NMR Spectroscopic Analysis Each insulin (14.7 mg) was dissolved in 140 μL of 0.1 N HCl, 70 μL of 0.1 N NaOH, 200 μL of Milli-Q water, 70 μL of 5 mM TSP/D_2O, and the pH was adjusted to 3.6 by adding aliquots of 0.1 N NaOH or HCl. Milli-Q water was added to give a total volume of 910 μL, and this mixture solution was diluted with 490 μL of CD_3CN. The solvent used in the present work was H_2O/D_2O : CD_3CN (65/35 vol%). For ^{1}H-NMR

* To whom correspondence should be addressed. e-mail: ako-ohno@nihs.go.jp
© 2012 The Pharmaceutical Society of Japan

Table 1. Each Insulin Mixture of the Sample Used in This Experiment: Human Insulin (A), Bovine Insulin (B), and Porcine Insulin (C)

Sample	A	:	B	:	C
A1	1		—		—
A4B1	4		1		—
A1B1	1		1		—
A1B4	1		4		—
B1	—		1		—
B4C1	—		4		1
B1C1	—		1		1
B1C4	—		1		4
C1	—		—		1
A1C4	1		—		4
A1C1	1		—		1
A4C1	4		—		1
A1B1C1	1		1		1
A2B1C1	2		1		1
A1B2C1	1		2		1
A1B1C2	1		1		2

measurements, a total sample volume of 700 μL with at least a 1.7 mM concentration (pH 3.6) was used.[13] Samples of each insulin mixture ratio are shown in Table 1.

The sample was introduced into an NMR test tube, and nuclear Overhauser effect spectroscopy (^{1}H-NOESY) spectra were recorded at 25°C using a Varian 600 MHz NMR spectrometer equipped with a cold probe. Thirty-two free induction decays (FIDs) with 75 K data points per FID were collected using a spectral width of 9615.4 Hz, an acquisition time of 4.00 s, and a total pulse recycle delay of 2.02 s. The water resonance was suppressed using presaturation during the first increment of the NOESY pulse sequence, with irradiation occurring during the 2.0 s relaxation delay and also during the 200 ms mixing time. Prior to Fourier transformation, the FIDs were zero-filled to 128 K and an exponential line broadening factor of 0.5 Hz was applied.[9,14] Spectral ^{1}H-NMR assignments were achieved according to the literature values of chemical shifts in various media.[13]

NMR Data Reduction and Preprocessing All ^{1}H-NMR spectra were phased and baseline corrected by Chenomx NMR Suite 6.0 software, professional edition (Chenomx Inc., Canada). ^{1}H-NMR spectra were subdivided into regions having an equal bin size of 0.04 ppm over a chemical shift range of 0.04—10.0 ppm (excluding the region around the water signal; 4.2—4.6 ppm), and the regions within each bin were integrated. The integrated intensities were then normalized to the total spectral area, and the data were converted from the Chenomx software format into Microsoft Excel format (*.xlt). The resulting data sets were then imported into SIMCA-P version 12.0 (Umetrics AB, Umeå, Sweden) for multivariate statistical analysis.

Multivariate Data Analysis PCA was performed to examine the intrinsic variation in the data sets. The quality of the models was described by the R^2x and Q^2 parameters, which indicate the proportion of variance in the data explained by the models and the goodness of fit. R^2x represents the goodness of fit of the PCA model, and Q^2 expresses the predictability of the PCA model. The quality of the PCA models was described by the total variance of principal component 1 (PC1) and principal component 2 (PC2) at a confidence level of 95%.

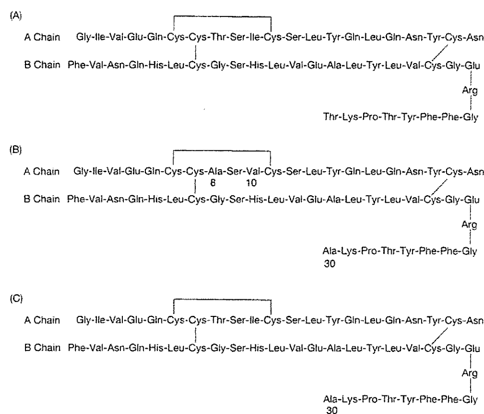

Fig. 1. Amino Acid Sequences of Human Insulin (A), Bovine Insulin (B), and Porcine Insulin (C)

Results

The amino-acid sequences of human, bovine, and porcine insulins are shown in Fig. 1. Bovine insulin differs from human insulin at the following positions: alanine (Ala) for threonine (Thr) at position A8 (8th position on the A Chain), valine (Val) for isoleucine (Ile) at A10, and Ala for Thr at the carboxyl terminus of the B-chain. Porcine insulin differs from human insulin with an Ala substituted for Thr at the carboxy terminus of the B-chain. ^{1}H-NMR spectra of the three types of insulin are shown in Fig. 2. While a simple visual inspection suggests that the three spectra might be indistinguishable, actual spectral differences may be detected if changes can be represented as points in a multidimensional space and examined using PCA. PCA of each insulin spectrum was performed, and distinct differences among the ^{1}H-NMR spectra at each sample mixture ratio were readily detected by the scores of both PC1 and PC2, which could be clearly depicted as points on the lines of the triangular phase diagram as shown in Fig. 3. In the PC1-PC2 plane, all samples were displayed in a triangular phase diagram bearing the three types of single composition insulin at each vertex. The cumulative contribution rate by PCA of the first two principal components, PC1 and PC2, was 63.8 and 83.3%, respectively. Thus, a spectrum change was characterized by PC1 and PC2 with species-related differences of insulin at a high contribution ratio. This result suggests a large contribution of human and bovine insulin to PC1, indicating that the positive direction from the center of the PC1 coordinate on the horizontal axis corresponded to bovine insulin and the negative direction corresponded to human insulin. Meanwhile, a high contribution to PC2 indicated that the positive direction from the center of the PC2 coordinate on the vertical axis corresponded to porcine insulin and the negative direction corresponded to human and bovine insulin. In addition, the mixed sample of all three types of insulin in a 1 : 1 : 1 ratio is in the center of the triangular phase diagram, and samples of each insulin mixture ratio radiate from the center toward each vertex.

The loading plot of all the evaluated ^{1}H-NMR signals is shown in Fig. 4. Each variable represents a peak at a particular chemical shift in the ^{1}H-NMR spectra shown in Fig.

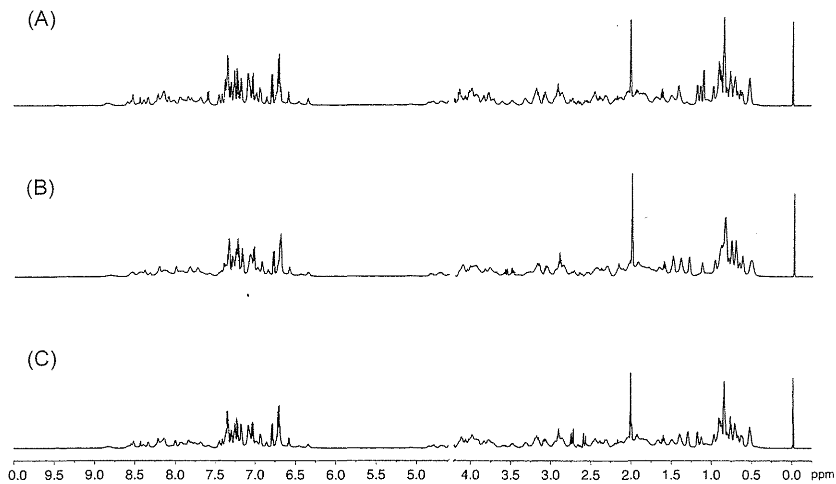

Fig. 2. ^{1}H-NMR Spectra of Human Insulin (A), Bovine Insulin (B), and Porcine Insulin (C)

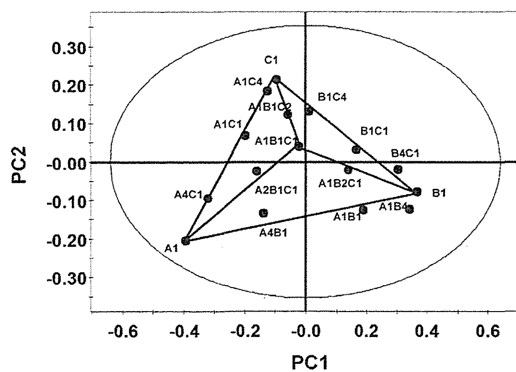

Fig. 3. PCA Scores Plot (PC1/2) Derived from the ^{1}H-NMR Spectral Data for Each Mixed Insulin Ratio

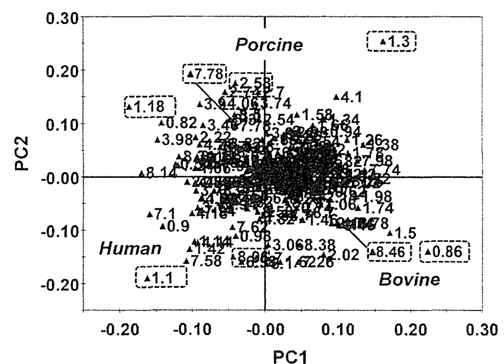

Fig. 4. The PCA Loading Plot (PC1/2) Derived from the ^{1}H-NMR Spectral Data for Each Mixed Insulin Ratio

1. This loading plot reveals the contributions of particular variables towards either an increase or decrease in the integrated intensities of the ^{1}H-NMR spectra. Six variables showing typical fluctuations of the different insulin species were identified (Fig. 4), and the integrated intensities of these variables corresponding to the insulin ratios are shown in Fig. 5. The tendency of the intensity of each of these variables to either increase or decrease is evident in the differences of the mixed insulin ratios and suggests specificity of the variables for the different insulin species. The corresponding characteristic variables of human, bovine, and porcine insulin were δ 1.1, 0.86 and 4.06 ppm, respectively. In addition, a common characteristic variable of bovine and porcine insulin occurred at δ 1.3 ppm and that of human and porcine insulin occurred at δ 1.18 ppm. The typical chemical shifts responsible for these variables were shown in Fig. 6. Therefore, these variables were indicative of the species specificity of insulin since the insulin species characterized by each variable tended to have a high intensity either for a single insulin species or for a species making up a high proportion of the mixture as shown in Fig. 5. Next, we examined whether the larger variables characterizing each species were derived from the type of amino acid residue by analysis of the loading and trend plots.

First, determination of the variables contributing significantly to the variation of the PC1 coordinate axis for the human and bovine insulin groups was performed by analysis of the amino acid residue peaks corresponding to these particular variables. Peaks for each variable could be identified: the variable at 1.1 ppm was attributed to both the γH of Ile at A10 and to the γH of Thr at B30; the variable of the amide group region at 8.06 ppm was attributed to the NH of Thr at A8 of the characteristic amino-acid sequences of human insulin. On the other hand, the variable at 0.86 ppm was attributed to the γH of Val at A10; and the variable at 1.5 ppm was attributed to the βH of Ala at A8 and/or B30; the variable of the amide group region at 8.46 ppm was attributed to the NH of Val at A10 of the characteristic amino-acid sequences of bovine insulin.

Next, determination of the variables contributing significantly to the variation of the PC2 coordinate axis for the two groups, porcine, and both human and bovine was performed by the analysis of the amino acid residue peaks corresponding to these particular variables. Peaks for each variable could be identified: the variable at 4.06 ppm was attributed to the αH of Ala at B30; the variable of the amide group region at 7.78 ppm was attributed to the NH of Ala at B30 of the characteristic amino-acid sequences of porcine insulin. Therefore, identified amino acids for each characteristic variable were by inference associated with the primary structure of the three types of

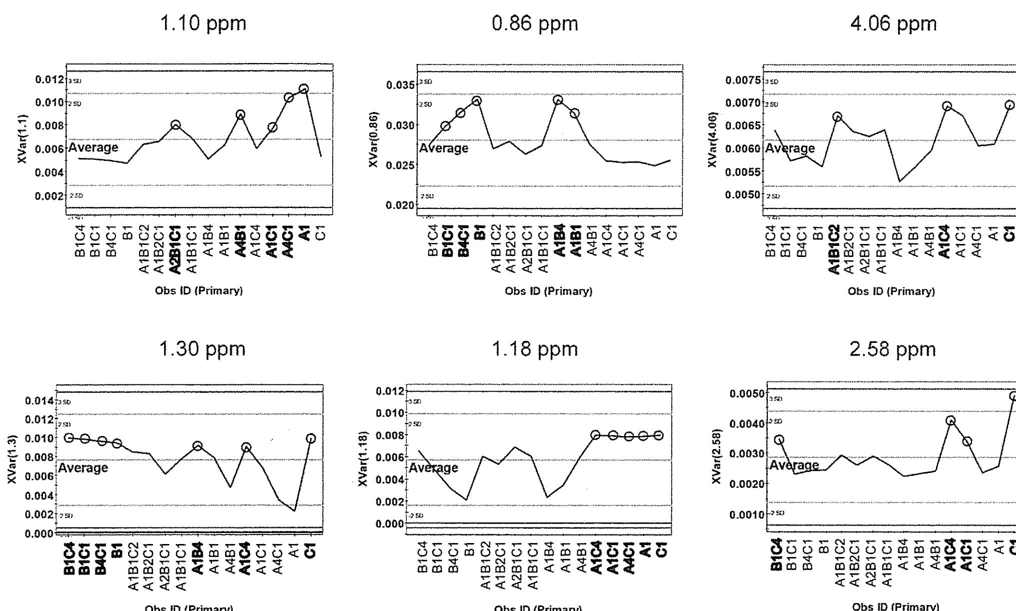

Fig. 5. The PCA Trend Plot: Integrated Intensities of Six Variables Showing Typical Fluctuations of Human Insulin, Bovine Insulin, and Porcine Insulin on the Loading Plot

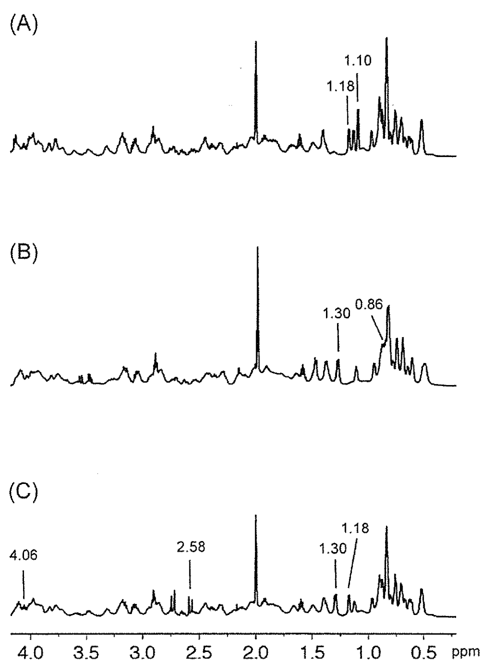

Fig. 6. The Typical Chemical Shifts for the Different Insulin Species on the PCA Loading Plot: Human (A), Bovine (B), and Porcine (C)

insulin, as shown in Fig. 4.

Discussion

The three insulin species used in this study each consist of 51 amino acid residues; bovine insulin has three different positions and porcine insulin has one different position from human insulin. In general, it is extremely difficult to distinguish differences of one to three amino acid residues in the ^{1}H-NMR spectrum of polypeptides of approximately MW 6000. However, we succeeded in distinguishing between the insulin species using a combination of multivariate statistics and ^{1}H-NMR spectra. PCA of the insulin spectrum for each mixture ratio was performed, and variables due to several different amino acid residues were detected from both the scores of PC1 and PC2, clearly depicting three separate groups, as shown in Figs. 3 and 4. In addition, from the scores plot, the components of the single insulin species and of mixtures consisting of two-three species were statistically distributed in the triangular phase diagram according to differences in the species composition ratio (Fig. 3, Table 1). This result shows that it is possible to analyze the composition of a mixture of species with a small number of amino acid sequence differences by taking advantage of the scores plot.

We also examined by PCA the partial aliphatic and amide regions of each insulin spectrum (data not shown). The determination of the variables contributing significantly to the variation of the PC1 coordinate axis for the human and bovine insulin groups and to the variation of the PC2 coordinate axis for the two groups, porcine, and both human and bovine insulin groups of the loading plots was performed by analysis of the amino acid residue peaks corresponding to these particular variables. Differences of the characteristic amino acid residues for each insulin species as well as the results from analyzing entire spectra were reflected in the scores plot. It is noteworthy that a similar tendency from analysis of the complete spectral region was observed with the scores plot of the amide region. These results suggest that it may be possible to distinguish slight sequence differences of polypeptides by PCA analysis of the amide region of the NMR spectrum.

On the other hand, the biological effect of polypeptides is also influenced by differences in their higher-order structure. It is difficult to evaluate differences in the higher-order structure of polypeptides by conventional analytical methods. In this PCA analysis study, it was found that the first and second principal components accounted for a majority of the vari-

ability differences of the primary insulin species structures. Interestingly, there were some variables that were not derived from the differences of amino acids among the three insulin types. Through a comparison of the NOESY spectra of the insulin species, it was proposed that these variables were associated with differences in the higher-order structures (data not shown). Therefore, the NMR technique coupled with PCA might also be useful as a tool for analyzing the higher-order structure, which is associated with the quality of a polypeptide, because in addition to primary structure information of the amino acid residues, the ^{1}H-NMR spectrum also contains information related to the three-dimensional structure of a molecule that is dependent on the solution conformation.

In conclusion, we have succeeded in precisely characterizing samples of human, bovine, and porcine insulin, molecules that differ in amino acid sequence from one to three amino acid residues, by ^{1}H-NMR spectroscopy coupled with PCA. Currently, assessment of the differences of higher-order structure using PCA analysis of NOESY spectral data are underway.

Acknowledgements We thank Dr. J. Kurita and Mr. K. Kushida (Agilent Technologies Japan Ltd.) for their technical assistance in measuring the NMR spectra. This work was supported by a Health Labour Sciences Research Grant from the Ministry of Health, Labour, and Welfare, Japan and by a 'Grant-in-Aid for Young Scientists (B)' (No. 22790126) from the Ministry of Education, Culture, Sports, Science and Technology (MEXT) of Japan.

References

1) Eriksson L., Johansson E., Kettaneh-Wold N., Wold S., "Multi- and Megavariate Data Analysis," Umetrics Academy, Umeå, 2001.
2) Wold S., Albano C., Dunn W. J., Edlund U., Esbensen K., Geladi P., Hellburg S., Johansson E., Lindberg W., Sjostrom M., "Chemometrics: Mathematics and Statistics in Chemistry," D. Reidel Publishing Company, Dordrecht, 1984.
3) Clayton T. A., Baker D., Lindon J. C., Everett J. R., Nicholson J. K., *Proc. Natl. Acad. Sci. U.S.A.*, **106**, 14728—14733 (2009).
4) Clayton T. A., Lindon J. C., Cloarec O., Antti H., Charuel C., Hanton G., Provost J. P., Le Net J. L., Baker D., Walley R. J., Everett J. R., Nicholson J. K., *Nature* (London), **440**, 1073—1077 (2006).
5) Coen M., Holmes E., Lindon J. C., Nicholson J. K., *Chem. Res. Toxicol.*, **21**, 9—27 (2008).
6) Crockford D. J., Holmes E., Lindon J. C., Plumb R. S., Zirah S., Bruce S. J., Rainville P., Stumpf C. L., Nicholson J. K., *Anal. Chem.*, **78**, 363—371 (2006).
7) Fukuhara K., Ohno A., Ando Y., Yamoto T., Okuda H., *Drug Metab. Pharmacokinet.*, **26**, 399—406 (2011).
8) Ohno A., Kawasaki N., Fukuhara K., Okuda H., Yamaguchi T., *Chem. Pharm. Bull.*, **57**, 1396—1399 (2009).
9) Ohno A., Oka K., Sakuma C., Okuda H., Fukuhara K., *J. Agric. Food Chem.*, **59**, 5181—5187 (2011).
10) Pongsuwan W., Bamba T., Yonetani T., Kobayashi A., Fukusaki E., *J. Agric. Food Chem.*, **56**, 744—750 (2008).
11) Uchiyama M., Toyoshima S., Ono S., Uyama Y., "Iyakuhin Hyouka Gaisetu," Tokyo Kagaku Doujin, Tokyo, 2009.
12) Ohno A., Kawasaki N., Fukuhara K., Okuda H., Yamaguchi T., *Magn. Reson. Chem.*, **48**, 168—172 (2010).
13) Bocian W., Sitkowski J., Bednarek E., Tarnowska A., Kawecki R., Kozerski L., *J. Biomol. NMR*, **40**, 55—64 (2008).
14) Nicholson J. K., Foxall P. J., Spraul M., Farrant R. D., Lindon J. C., *Anal. Chem.*, **67**, 793—811 (1995).

Rapid and Sensitive Method for Measuring the Plasma Concentration of Doxorubicin and Its Metabolites

Kumiko Sakai-Kato,*[a] Kunie Nanjo,[a] Toru Kawanishi,[b] and Haruhiro Okuda[a]

[a] *Division of Drugs, National Institute of Health Sciences; and* [b] *National Institute of Health Sciences; 1–18–1 Kamiyoga, Setagaya-ku, Tokyo 158–8501, Japan.*
Received September 9, 2011; accepted December 16, 2011; published online December 21, 2011

Doxorubicin is an anti-cancer drug with a wide therapeutic range. However, it and its metabolites cause severe side effects, limiting its clinical use. Therefore, measuring the plasma concentration of doxorubicin and its metabolites is important to study the dosing regimen of doxorubicin. We developed a rapid and sensitive method by ultra-high-performance liquid chromatography with fluorescent detection for measuring the plasma concentration of doxorubicin and its metabolites in small volumes (around 10 μL), enabling repeated measurements from the same mouse. The sensitivity of 7-deoxydoxorubicinolone, a major metabolite of doxorubicin, increased about 5 times than those ever reported using conventional HPLC, and the run time was within 3 min. The area under the curve ($AUC_{0-24\,h}$) of doxorubicin was 5.9 μg h/mL similar to the value of 4.16 μg h/mL obtained previously using a conventional HPLC method. This method would provide information that could be used to refine the therapeutic approach to doxorubicin use.

Key words doxorubicin; metabolite; pharmacokinetics

The anthracycline doxorubicin is one of the most widely used anticancer agents, and it has a broad spectrum of activity against a variety of malignancies.[1,2] New formulation technologies to enhance the effectiveness and safety of this anticancer drug are currently being developed. For instance, long-circulating and sterically stabilized liposomes containing doxorubicin can markedly increase tumor-specific deposition of drugs and have been approved as clinical products.[3] However, the clinical use of doxorubicin is limited by the side effect of cumulative, dose-dependent, irreversible chronic cardiomyopathy caused by doxorubicin itself and its metabolites, and optimal dose schedules remain a matter of debate.[4] Therefore, measuring the plasma concentration of doxorubicin and its metabolites is important to study the dosing regimen of doxorubicin.

Mice are very useful small laboratory animals for nonclinical research and are often used for pharmacokinetic, pharmacological, or drug formulation studies of doxorubicin.[5—7] Blood collection from the tail vein is becoming popular from the perspective of animal protection, but it has the limitation of small sample volumes. Therefore, it is often difficult to perform repeat investigations in the same animal to assess time-dependent changes in plasma concentrations, and many mice have to be killed for whole blood collection at each time point.

In a previous study, we succeeded in developing a method for measuring intracellular concentrations of doxorubicin and its metabolites by using ultra-high-performance liquid chromatography (UHPLC).[8] The resolution, sensitivity, and speed of analysis dramatically increased with the use of 2-μm particles in the stationary phase, high linear velocities for the mobile phase, and instrumentation that operates at higher pressures than those used in HPLC.[9—11] Specifically, the quantitation limit of doxorubicin was about 2 times lower than the limit ever reported using conventional HPLC, and run time was shorten from 20 min to within 3 min.[12,13] Because of the high sensitivity of our method and the small sample volumes (around 10 μL) required, in the current study we were able to measure changes in the concentration of doxorubicin and its metabolites over time in a single mouse, thereby diminishing the number of animals needed. This method would also have clinical utility, because the reduction of sample volumes and analytical times would decrease the burden of therapeutic drug monitoring (TDM) for patients.

Experimental

Drugs and Chemicals Doxorubicin hydrochloride, daunorubicin hydrochloride, and verapamil were purchased from Wako Pure Chemical Industries, Ltd. (Osaka, Japan). Doxorubicinol hydrochloride, and 7-deoxydoxorubicinolone were purchased from Toronto Research Chemicals Inc. (North York, Canada). Doxorubicinolone was synthesized from doxorubicinol by acidic hydrolysis (0.5 N HCl) at 50°C for 24 h, and then extracted with chloroform by a liquid–liquid extraction method.[14] Stock solution of each chemical was prepared by weighing separately. The primary stock solution of each chemical was prepared in methanol at 0.35 or 0.1 mg/mL and stored at −80°C. The standard solutions for validation data were obtained by mixing each chemical with mouse blank plasma.

Preparation of Mouse Plasma Samples for HPLC Doxorubicin was administered at 10 mg/kg by tail vein injection into female Balb/c mice purchased from CLEA Japan, Inc. (Tokyo, Japan). Blood was collected from the tail vein into heparinized capillaries 10, 20, 40, and 60 min and 2, 6, and 24 h after doxorubicin administration. Plasma obtained from the blood sample (about 10 μL) was mixed with saline, 50% methanol, and $ZnSO_4$ (final concentration: 400 mg/mL) and centrifuged at 15000 *g* for 10 min in a microcentrifuge (Model 3740, Kubota Corp., Tokyo, Japan); the supernatants were then collected. Plasma and saline volumes were adjusted so that the concentration of each compound was within the calibration curve range. A 15-μL aliquot of each supernatant was mixed with 5 μL of the internal standard (daunorubicin, 10 μg/mL in methanol), 22.5 μL ice-cold methanol, and 7.5 μL Milli-Q water, and filtered through a 0.20-μm filter (Millex-LG, Millipore Corp., Tokyo, Japan). The filtrates were transferred to autosampler vials before UHPLC analysis. All experimental procedures were approved by the institutional

* To whom correspondence should be addressed. e-mail: kumikato@nihs.go.jp © 2012 The Pharmaceutical Society of Japan

animal care and use committee.

HPLC Conditions High-throughput quantification of doxorubicin and its metabolites was performed in a Hitachi LaChrom ULTRA system equipped with an L-2160U pump, an L-2200U automated sample injector, an L-2300 thermostatted column compartment, and an L-2485U fluorescence detector (Hitachi, Tokyo, Japan).[8]

Samples were analyzed on a Capcell Pak C18 IF column (2.0×50 mm; particle size, 2 μm; Shiseido Corp., Tokyo, Japan). The mobile phase consisted of a mixture of 50 mM sodium phosphate buffer (pH 2.0) and acetonitrile (65 : 27, v/v). The mobile phase was delivered at a rate of 300 μL/min, and the column temperature was maintained at 25°C. The fluorescence detector was operated at an excitation wavelength of 470 nm and an emission wavelength of 590 nm.

Pharmacokinetics Analysis Pharmacokinetics were analyzed by noncompartmental analysis using Phoenix WinNonlin V6.1 software (Pharsight Corporation, CA, U.S.A.).

Results and Discussion

Doxorubicin is mainly metabolized in liver, and the estimated metabolic pathway was shown in Fig. 1a. According to a report where human metabolism of doxorubicin was studied

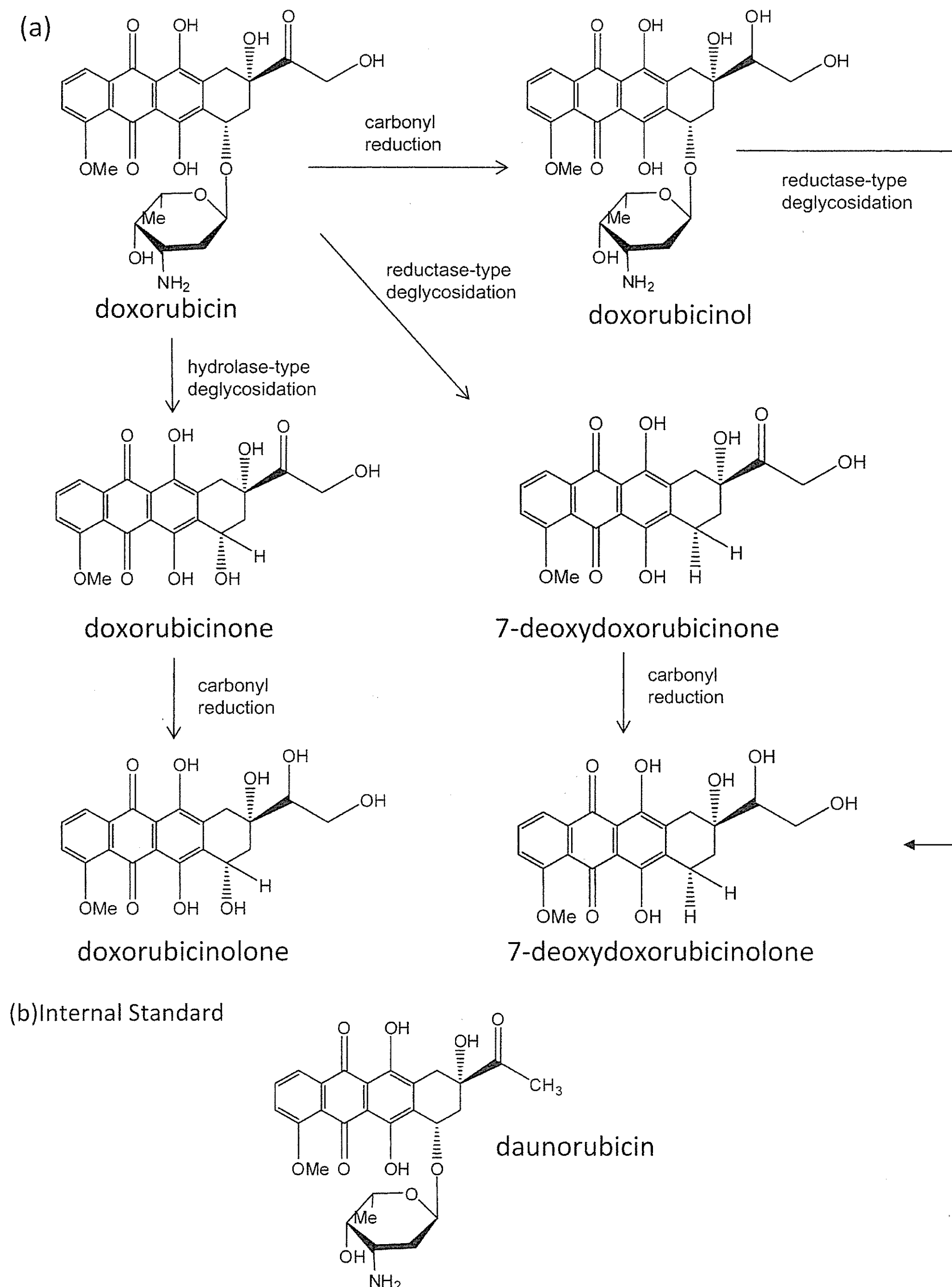

Fig. 1. Schematic Showing the Chemical Structures of Doxorubicin and Its Metabolites (a) and the Chemical Structure of Daunorubicin, the Internal Standard (b)

Table 1. Linearity of Doxorubicinone and Its Metabolites

	Slope			Intercept		r^2
	Mean	S.D.	Precision (%)	Mean	S.D.	
Doxorubicinol	12.71	0.22	1.73	0.0012	0.0062	1.000
Doxorubicin	12.16	0.19	1.56	−0.0009	0.0026	1.000
Doxorubicinolone	10.89	0.22	2.04	0.0029	0.0073	0.999
7-Deoxydoxorubicinolone	14.07	0.31	2.20	0.0049	0.0069	0.999

Precision (%): expressed as % R.S.D. (S.D./mean)×100.

Table 2. Detection Limit and Quantification Limit of Doxorubicin and Its Metabolites

	Doxorubicinol	Doxorubicine	Doxorubicinolone	7-Deoxydoxorubicinolone
Detection limit (pg)	3.8	4.9	6.4	7.4
Quantification limit (pg)	12.8	16.4	21.4	24.5

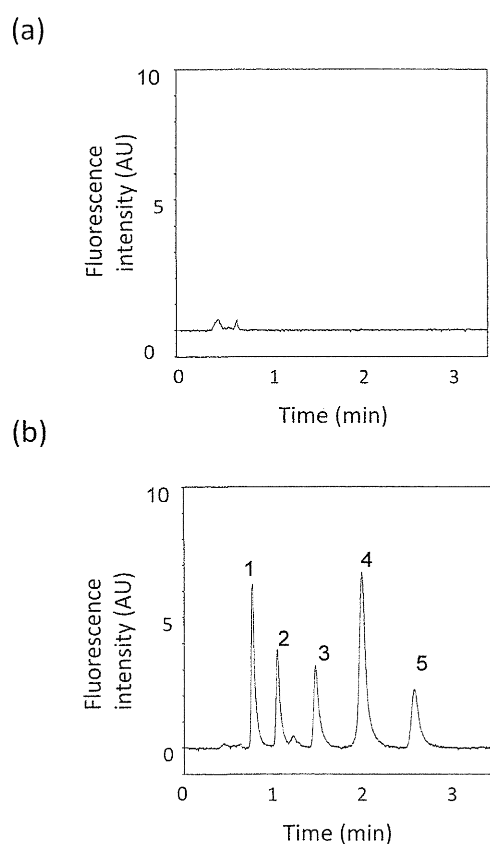

Fig. 2. Chromatograms of (a) Mouse Plasma and (b) Mouse Plasma Spiked with Doxorubicin and Its Metabolites

The chromatographic conditions are described in Experimental. AU; Arbitrary units. 1, doxorubicinol; 2, doxorubicin; 3, doxorubicinolone; 4, daunorubicin (internal standard); 5, 7-deoxydoxorubicinolone.

by isolating and identifying urinary metabolites, the metabolites retained doxorubicin's specific fluorescence properties.[15] Therefore, in this report, we used the fluorescent detection condition optimized for doxorubicin. Although the metabolites in human urine contained sulfate and glucuronide conjugates, which conjugate reactions also occur in liver, these conjugates were not detected in mouse plasma in our study. When a standard solution of doxorubicin, doxorubicinol, doxorubicinolone, 7-deoxydoxorubicinolone, and an internal standard (daunorubicin (Fig. 1b)) was analyzed, all compounds were separated within 3 min with good resolution (Fig. 2). The chromatogram of mouse plasma demonstrates the lack of chromatographic interference from endogenous plasma components (Fig. 2a). In a chromatogram of plasma spiked with doxorubicin and its metabolites at a concentration of 20 ng/mL, no interfering peaks were observed, and doxorubicin, the three metabolites, and the internal standard were well separated (Fig. 2b). These results show that the specificity of this method. We created calibration plots for doxorubicin and its metabolites. The plasma calibration curve was constructed using six calibration standards (2.5—100 ng/mL). The plots of relative peak area to IS *versus* concentration were linear over a wide range of concentrations (r^2=0.999—1.000) (Table 1). The detection limit and quantification limit were 3.8—7.4 pg and 12.8—24.5 pg injected compounds, respectively (signal to noise ratio, 3 : 1 for detection limits and 10 : 1 for quantitation limit). These values were 5 times lower than the limits ever reported using conventional HPLC[12,13,16—19] (Table 2).

We next tested the recovery of doxorubicin and its metabolites from mouse plasma spiked with each compound. The recovery rate was satisfactory, and the values for doxorubicinol, doxorubicin, doxorubicinolone, and 7-deoxydoxorubicinolone were 102.7, 92.6, 94.7, 96.7%, respectively (n=3). Tables 3 and 4 shows the accuracy and precision data for intra- and inter-day plasma samples. The assay values on both occasions (intra- and inter-day) were found to be within the accepted variable limits.[20]

The predicted concentrations for each analyte deviated within ±15% of the nominal concentrations in a series of stability test; in-injector (20 h), bench top (6 h), repeated three freeze/thaw cycles and at −80°C for at least 2 weeks (Table 5). Although 7-deoxydoxorubicinolone was slightly unstable under in-injector (20 h; 91.24%), other compounds were stable at any storage conditions.

We then used the validated method described above for the simultaneous detection of doxorubicin and its metabolites in mouse plasma after intravenous administration of doxorubicin. Doxorubicin and its metabolites doxorubicinol and 7-deoxydoxorubicinolone were detected in the plasma sample. Although doxorubicinolone has been also reported to be produced by NADP-dependent cytochrome P450 reductase,[13,15] it was not detected in this study (Fig. 3). Doxorubicinol is produced by cytosolic carbonyl reductase through the

Table 3. Intra-Day Assay Precision and Accuracy for Doxorubicin and Its Metabolites in Mouse Plasma

ng/mL	Doxorubicinol				Doxorubicin				Doxorubicinolone				7-Deoxydoxorubicinolone			
	Mean	S.D.	Precision	Accuracy	Mean	S.D.	Precision	Accuracy	Mean	S.D.	Precision	Accuracy	Mean	S.D.	Precision	Accuracy
5	5.12	0.41	8.08	102.45	4.98	0.15	3.03	99.56	4.82	0.61	12.73	96.30	4.70	0.44	9.42	93.90
25	25.16	1.40	5.55	100.63	25.46	0.88	3.47	101.84	23.56	1.39	5.92	94.24	25.75	1.25	4.84	102.99
100	99.78	0.94	0.94	99.78	99.55	0.99	1.00	99.55	99.49	1.21	1.22	99.49	99.47	1.13	1.14	99.47

Precision (%): expressed as % R.S.D. (S.D./mean)×100. Accuracy (%): calculated as (mean determined concentration/nominal concentration)×100.

Table 4. Inter-Day Assay Precision and Accuracy for Doxorubicin and Its Metabolites in Mouse Plasma

ng/mL	Doxorubicinol				Doxorubicin				Doxorubicinolone				7-Deoxydoxorubicinolone			
	Mean	S.D.	Precision	Accuracy	Mean	S.D.	Precision	Accuracy	Mean	S.D.	Precision	Accuracy	Mean	S.D.	Precision	Accuracy
5	5.13	0.16	3.04	102.51	5.35	0.49	9.18	107.05	5.31	0.35	6.55	106.18	4.95	0.11	2.25	98.95
25	24.31	0.68	2.81	97.24	23.74	0.38	1.59	94.96	24.84	0.42	1.69	99.34	24.56	0.37	1.52	98.24
100	99.83	0.48	0.48	99.83	100.11	1.13	1.13	100.11	100.39	0.32	0.32	100.39	99.83	0.44	0.44	99.83

Precision (%): expressed as % R.S.D. (S.D./mean)×100. Accuracy (%): calculated as (mean determined concentration/nominal concentration)×100.

Table 5. Stability Data in Mouse Plasma

	Doxorubicinol				Doxorubicin				Doxorubicinolone				7-Deoxydoxorubicinolone			
	Mean	S.D.	Precision	Accuracy	Mean	S.D.	Precision	Accuracy	Mean	S.D.	Precision	Accuracy	Mean	S.D.	Precision	Accuracy
5 ng/mL																
20 h (in-injector)	5.00	0.068	1.37	100.06	5.22	0.072	1.37	104.30	5.19	0.058	1.12	103.86	4.56	0.074	1.62	91.24
6 h (bench-top)	5.19	0.10	2.01	103.71	5.43	0.11	2.08	108.66	5.22	0.11	2.01	104.38	4.92	0.073	1.48	98.39
2 weeks at −80°C	4.72	0.12	2.43	94.36	5.23	0.14	2.62	104.54	5.21	0.082	1.58	104.20	4.98	0.092	1.84	99.59
3rd freeze-thaw	4.80	0.17	3.49	96.00	5.16	0.18	3.51	103.23	5.01	0.22	4.48	100.19	4.97	0.154	3.09	99.42
50 ng/mL																
20 h (in-injector)	51.27	1.48	2.89	102.53	54.10	2.07	3.82	108.20	47.08	1.54	3.28	94.16	50.69	1.77	3.49	101.38
6 h (bench-top)	53.78	2.90	5.39	107.55	52.12	2.76	5.30	104.25	49.66	2.27	4.56	99.32	54.33	2.36	4.33	108.66
2 weeks at −80°C	47.75	0.54	1.13	95.49	48.10	0.47	0.97	96.21	49.04	0.35	0.71	98.08	47.99	0.44	0.91	95.98
3rd freeze-thaw	52.09	0.81	1.56	104.18	51.04	0.81	1.59	102.08	48.68	0.95	1.96	97.37	51.52	0.86	1.68	103.04

Precision (%): expressed as % R.S.D. (S.D./mean)×100. Accuracy (%): calculated as (mean determined concentration/nominal concentration) ×100.

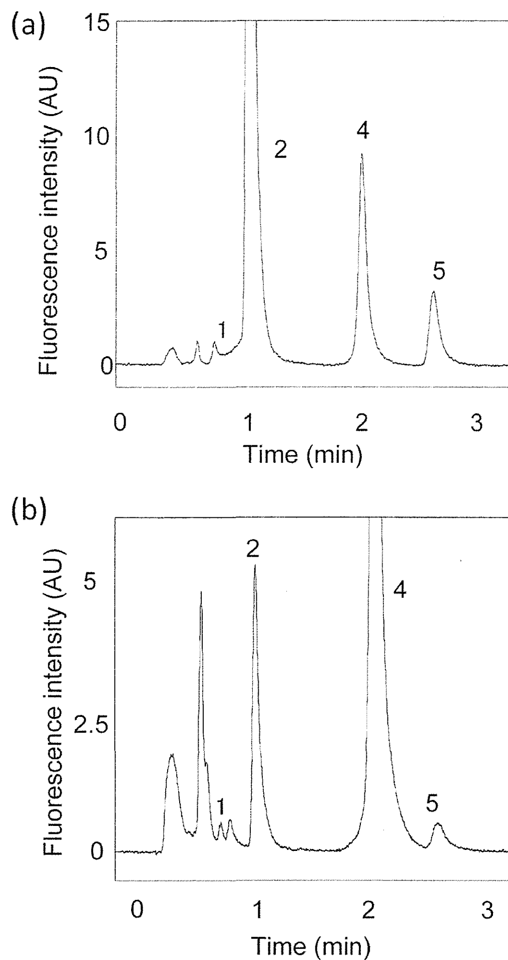

Fig. 3. Chromatogram of Mouse Plasma Obtained after Intravenous Administration of Doxorubicin

Doxorubicin (10 mg/kg) was administered by tail vein injection. Blood was removed from the tail vein after 10 min (a) and 6 h (b) of administration, and plasma was prepared as described in Experimental. 1, doxorubicinol; 2, doxorubicin; 4, daunorubicin (internal standard); 5,7-deoxydoxorubicinolone.

NADPH-dependent aldo-keto reduction of a carbonyl moiety in doxorubicin[15]; deglycosidation at the daunosamine sugar in doxorubicin or doxorubicinol produces 7-deoxydoxorubicinolone[15,21] (Fig. 1a). The major metabolites we detected were coincident with those reported previously.[22] We also examined the time course of changes in the concentrations of doxorubicin and its metabolites (Fig. 4a). After an initial rapid decrease, the doxorubicin concentration decreased slowly, and the plasma concentration of doxorubicin was 74.2 ng/mL (6 h) and 61.1 ng/mL (24 h) (n=3). The persistence of doxorubicin indicates that doxorubicin comes back very slowly from some distributed tissues or circulates for a relatively long time by binding to plasma proteins.[15]

The area under the curve ($AUC_{0-24\,h}$) and C_{max} of doxorubicin was 5.9 μg h/mL and 10.0 μg/mL, respectively, similar to the value of 4.16 μg h/mL, and 5.4 μg/mL obtained previously using a conventional HPLC method.[7] In addition, our method enabled us to trace the change in doxorubicin concentration over time in a single mouse (Fig. 4b); this had previously been difficult to do because of the small sample volumes. This property will allow us to minimize the number of animals

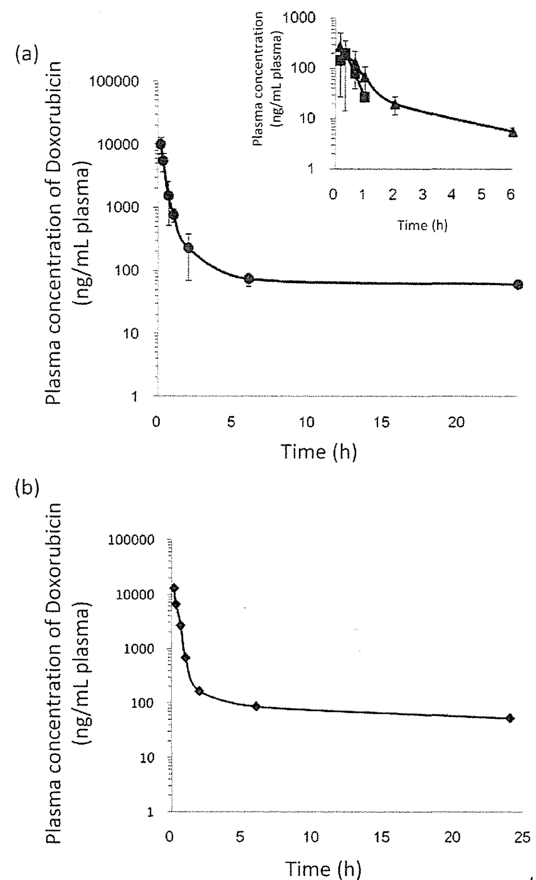

Fig. 4. Changes in Plasma Concentration over Time

Blood was collected from tail veins 10, 20, or 30 min or 1, 2, 6, or 24 h after administration of doxorubicin, and the drug concentrations in the plasma were measured. (Averaged results from 3 mice (a) and result of one mouse (b).) Main graph, doxorubicin. Inset, metabolites (squares: doxorubicinol; triangles: 7-deoxydoxorubicinolone).

needed for pharmacokinetic analyses. Furthermore, in a clinical setting, the small blood sample volumes and fast analytical time would reduce the impact of TDM on patients.

Conclusions

Our results show that the method we developed using UHPLC provides rapid analysis using very small plasma samples. The method is sensitive enough to evaluate changes in the concentrations of doxorubicin and its metabolites in a single mouse; this will result in the use of smaller numbers of animals, which is good for animal protection. In clinical applications, this method could also decrease the burden of TDM for patients. We predict that it will greatly facilitate studies of doxorubicin pharmacokinetics and clarify the effect of doxorubicin metabolism on therapeutic outcome.

Acknowledgements The authors are grateful for financial support from the Research on Publicly Essential Drugs and Medical Devices Project (The Japan Health Sciences Foundation); a Health Labor Sciences Research Grant from the Ministry of Health, Labour, and Welfare (MHLW); and KAKENHI (21790046) from the Ministry of Education, Culture, Sports, Science and Technology (MEXT) of Japan.

References

1) Hortobágyi G. N., *Drugs*, **54** (Suppl. 4), 1—7 (1997).
2) Di Marco A., Gaetani M., Scarpinato B., *Cancer Chemother. Rep.*, **53**, 33—37 (1969).
3) O'Brien M. E., Wigler N., Inbar M., Rosso R., Grischke E., Santoro A., Catane R., Kieback D. G., Tomczak P., Ackland S. P., Orlandi F., Mellars L., Alland L., Tendler C., CAELYX Breast Cancer Study Group, *Ann. Oncol.*, **15**, 440—449 (2004).
4) Olson R. D., Mushlin P. S., Brenner D. E., Fleischer S., Cusack B. J., Chang B. K., Boucek R. J. Jr., *Proc. Natl. Acad. Sci. U.S.A.*, **85**, 3585—3589 (1988).
5) van Asperen J., van Tellingen O., Beijnen J. H., *Drug Metab. Dispos.*, **28**, 264—267 (2000).
6) Yokoyama M., Okano T., Sakurai Y., Fukushima S., Okamoto K., Kataoka K., *J. Drug Target.*, **7**, 171—186 (1999).
7) Nakanishi T., Fukushima S., Okamoto K., Suzuki M., Matsumura Y., Yokoyama M., Okano T., Sakurai Y., Kataoka K., *J. Controlled Release*, **74**, 295—302 (2001).
8) Sakai-Kato K., Saito E., Ishikura K., Kawanishi T., *J. Chromatogr. B Analyt. Technol. Biomed. Life Sci.*, **878**, 1466—1470 (2010).
9) Swartz M. E., *J. Liq. Chrom. Rel. Technol.*, **28**, 1253—1263 (2005).
10) Nováková L., Vlcková H., *Anal. Chim. Acta*, **656**, 8—35 (2009).
11) Sun N., Lu G., Lin M., Fan G., Wu Y., *Talanta*, **78**, 506—512 (2009).
12) van Asperen J., van Tellingen O., Beijnen J. H., *J. Chromatogr. B Biomed. Sci. Appl.*, **712**, 129—143 (1998).
13) Zhou Q., Chowbay B., *J. Pharm. Biomed. Anal.*, **30**, 1063—1074 (2002).
14) Maudens K. E., Stove C. P., Lambert W. E., *J. Sep. Sci.*, **31**, 1042—1049 (2008).
15) Takanashi S., Bachur N. R., *Drug Metab. Dispos.*, **4**, 79—87 (1976).
16) Andersen A., Warren D. J., Slørdal L., *Ther. Drug Monit.*, **15**, 455—461 (1993).
17) Shinozawa S., Mimaki Y., Araki Y., Oda T., *J. Chromatogr.*, **196**, 463—469 (1980).
18) Rose L. M., Tillery K. F., el Dareer S. M., Hill D. L., *J. Chromatogr.*, **425**, 419—423 (1988).
19) Andersen A., Holte H., Slørdal L., *Cancer Chemother. Pharmacol.*, **44**, 422—426 (1999).
20) Guidance for Industry: Bioanalytical Method Validation. U.S. Department of Health and Human Services Food and Drug Administration (2001)
21) Lown J. W., *Pharmacol. Ther.*, **60**, 185—214 (1993).
22) van Asperen J., van Tellingen O., Tijssen F., Schinkel A. H., Beijnen J. H., *Br. J. Cancer*, **79**, 108—113 (1999).

Comparison of Particle Size and Dispersion State among Commercial Cyclosporine Formulations and Their Effects on Pharmacokinetics in Rats

Hiroko Shibata,* Haruna Saito, Toru Kawanishi, Haruhiro Okuda, and Chikako Yomota

National Institute of Health Sciences; 1–18–1 Kamiyoga, Setagaya-ku, Tokyo 158–8501, Japan.
Received February 13, 2012; accepted May 18, 2012

Generic versions of Neoral, a microemulsion capsule formulation of cyclosporine, have been approved worldwide. However, there are concerns about the quality and efficacy of the generics due to the formulation specificity and differences in inactive ingredients among products. In this study, we measured the physicochemical properties of both the innovator and the generic formulations, and compared their bioavailability in rats. When the capsule contents were dispersed in water, the absorbance (600 nm wavelength) of generic products was higher than that of the innovator. Whereas the dispersion solution of the innovator in Fed State Simulated Intestinal Fluid was nearly clear, that of all the generics became white and turbid. The mean diameter of the microemulsion (or emulsion) formed in water by the generics was 39.7, 57.7, 64.5, and 74.8 nm, all of which were larger than that of the innovator (26.4 nm). Although the T_{max} of the generics tended to be long relative to that of the innovator, there were no significant differences between the innovator and generics with regard to maximum blood concentration (C_{max}) or area under the curve (*AUC*). These results suggest that the physicochemical differences between the innovator and the generics will not have a significant effect on C_{max} or *AUC*, which is necessary to ensure bioequivalence.

Key words microemulsion; emulsion; biorelevant medium; innovator; generic

Cyclosporine (CsA) is an immunosuppressive agent,[1,2] and is categorized as a Biopharmaceutics Classification System (BCS) Class II drug with high lipophilicity[3] and low aqueous solubility.[4] One way to improve the aqueous solubility of such drugs is to prepare them as self-emulsifying formulations.[5,6] The first generation of orally administered formulations containing CsA consisted of a corn-oil-based solution encapsulated in soft gelatin (Sandimmune), which is now referred to as a "self-emulsifying drug delivery system" (SEDDS). The oily solutions are emulsified by bile salts, which form mixed micelles in the gastrointestinal fluid, and the CsA in these mixed micelles is then absorbed from the upper intestinal tract.[7] Thus, the absorption of CsA in Sandimmune is susceptible to the effects of bile acid secretion and the ingestion of food, resulting in variability of absorption within individual patients.[8,9]

To address the variability in absorption of Sandimmune, an improved formulation of CsA, Neoral, has been developed. Neoral is a microemulsion pre-concentrate formulation, which has recently been referred to as a "self-microemulsifying drug delivery system" (SMEDDS).[6] After oral administration of Neoral, a microemulsion with stable dispersibility is easily formed in the intake water or gastric fluid, and the drug is quickly absorbed from the upper intestinal tract. Therefore, when compared to Sandimmune, Neoral demonstrates a significantly higher and more consistent absorption profile that is unaffected by bile acid secretion or food consumption.[10–12]

The need to reduce healthcare costs in many countries has led to the production of generic substitutions for original drugs. Four generic versions of Neoral have already been approved in Japan; in other countries, several generics have been marketed, such as Gengraf, Eon, and Cicloral. In the U.S.A., SangCya, which is the liquid generic form of Neoral, was recalled because it is not bioequivalent to Neoral when administered with apple juice.[13] There are reports that in transplant recipients the area under the curve (*AUC*) and maximum blood concentration (C_{max}) values of the generic tended to be lower than those of the innovator, and that the bioavailability of the innovator decreased when administered after a fat-rich meal, whereas that of the generic increased.[14,15] A recent report at a scientific meeting in Japan also indicated that the physical appearance and particle diameter of generics were different from those of the innovator.[16] In addition, another group reported that after oral administration in rats, the pharmacokinetics of CsA metabolites differed between the innovator and generics.[17]

Thus, as we describe above, there are concerns about the quality and efficacy of generics due to the formulation specificity of the innovator and the narrow therapeutic window of CsA. To our knowledge, there have been no direct comparisons of innovator and generics using both *in vitro* and *in vivo* assessment. Therefore, in this study, we assessed the physicochemical properties of various commercial formulations of CsA when dispersed in solution, such as their physical appearance and particle diameter. We examined the oil-based formulation Sandimmune, the microemulsion formulation Neoral, and 4 generic products of Neoral that are approved by the regulatory agency in Japan. In addition, we compared the pharmacokinetics of CsA and its metabolites for these formulations, and investigated whether or not the differences in physicochemical properties are likely to affect their pharmacokinetics.

Experimental

Materials Six cyclosporine A (CsA) capsule products were purchased from a general sales agency for drugs in Japan and used in this study: Sandimmune® capsule, 50 mg (Product A, Lot No. S0016; Novartis Pharma K.K., Basel,

The authors declare no conflict of interest.

* To whom correspondence should be addressed. e-mail: h-shibata@nihs.go.jp
© 2012 The Pharmaceutical Society of Japan

Switzerland); Neoral® capsule, 50 mg (Product B, Lot No. S1046; Novartis Pharma K.K., Basel, Switzerland); Amadora® capsule, 50 mg (Product C, Lot No. 34006; TOYO CAPSULE Co., Ltd., Shizuoka, Japan); Cicporal® capsule, 50 mg (Product D, Lot No. EC2501; Nichi-Iko Pharmaceutical Co., Ltd., Toyama, Japan); cyclosporine capsule, 50 mg "Mylan" (Product E, Lot No. 0450RH; Mylan Seiyaku, Tokyo, Japan); and cyclosporine capsule, 50 mg "FC" (Product F, Lot No. 9C1; Fuji Capsule Co., Ltd., Shizuoka, Japan). The official CsA reference standard was purchased from the Phramaceutical and Medical Device Regulatory Science Society of Japan. Sodium taurocholate and lecithin were purchased from Wako Pure Chemical Industries (Osaka, Japan). Cyclosporin D (CsD) (ALEXIS® Biochemicals) was purchased from Enzo Life Sciences (Farmingdale, NY, U.S.A.). Rat liver microsomes were obtained from Celsis In Vitro Technologies (Baltimore, MD, U.S.A.). β-Nicotinamide-adenine dinucleotide phosphate (NADP), glucose-6-phosphate 1-dehydrogenase (G-6-PDH), and glucose-6-phosphate (G-6-P) were purchased from Oriental Yeast Co., Ltd. (Tokyo, Japan).

Physicochemical Characteristics Eighty percent of the contents of a single capsule was placed in a test tube, and 10 mL of test medium was added. The solution was mixed by gentle inversion until the capsule contents were dispersed homogeneously in the test medium. Using this solution, 5-fold and 25-fold dilutions were prepared in different test tubes.

Preparation of Test Medium The 1st Fluid and 2nd Fluid for the dissolution test were prepared according to the Japanese Pharmacopoiea (JP)16. Fasted State Simulated Intestinal Fluid (FaSSIF) and Fed State Simulated Intestinal Fluid (FeSSIF) were prepared by the modified method reported by Galia *et al.* and Jantratid *et al.*[18,19] FaSSIF was formulated using approximately 900 mL of blank buffer, which was prepared by dissolving sodium chloride (4.01 g), sodium hydrate (1.39 g), and maleic acid (2.22 g) in 900 mL distilled water. The pH was then adjusted to 6.5. Sodium taurocholate (1.613 g) was dissolved in 50 mL of blank buffer, to which lecithin (0.15 g) was added and dissolved with heat and agitation until the solution became clear. The volume was adjusted to 1 L using the remaining blank buffer and distilled water. In the case of FeSSIF, sodium taurocholate (8.07 g) was dissolved in 50 mL of blank buffer (potassium chloride [15.20 g] and acetate [8.65 g] in 900 mL distilled water, pH 5.0), to which lecithin (2.81 g) was added and dissolved with heat and agitation until the solution became clear and yellow. The volume was adjusted to 1 L as with FaSSIF. Mixed micelles were not detected in either FaSSIF or FeSSIF when examined by a dynamic light scattering (DLS) photometer.

Absorbance To assess the degree of turbidity, the absorbance at 600 nm of each capsule sample was measured by a spectrophotometer (UV-2550/2450; Shimadzu, Kyoto, Japan) after mixing the samples with different test media.

Solubility The solubility of CsA in the dispersed solution was measured. The dispersed solution of each capsule sample was filtrated by 0.45 μm filter, and its concentration of CsA was measured by HPLC. The apparatus used for the HPLC system consisted of a constant pump (L-7200, Hitachi High-Technologies Corporation, Tokyo, Japan), a degasser (L-7610, Hitachi), an autoinjector (L-7200, Hitachi), a column oven (L-7300, Hitachi), an UV detector (214 nm) (L-7405, Hitachi), and a system controller (D-7000, Hitachi). The separation was carried out at 70°C on a Inertsil ODS-3 (100×4.0 mm i.d., 5 μm) from GL Science (Tokyo, Japan). The mobile phase consisted of water–tetrahydrofuran (5 : 3.6), and flow rate was 1.0 mL/min. A standard stock solution of CsA was prepared by dissolving 10 mg of CsA in 10 mL of ethanol, and stored at 4°C. A 10 μL aliquot of a sample was injected.

Particle Size Distribution The size distribution and mean diameter of particles in the capsule content samples were measured using a DLS photometer DLS-7000 (Otsuka Electronics Co., Ltd., Osaka, Japan) equipped with an He–Ne laser source (wavelength, 632.8 nm) after mixing the samples with different test media. All DLS measurements were made with a scattering angle of 90°. The neutral density filter was adjusted depending on intensity. Data were gathered with a counting period of 100 s. Histogram analysis was performed to assess the particle size distribution, and cumulant analysis was performed to calculate the mean diameter. The data between different products were statistically analyzed using a one-way analysis of variance followed by Dunnett's test.

The number of large-diameter particles (>0.5 μm) in the solution of the capsule content in 10 mL water was measured by an Accusizer 780A instrument (Particle Sizing Systems, Santa Barbara, CA, U.S.A.). This instrument is based on light extinction (LE) or light scattering (LS) that employs a single-particle optical sizing (SPOS) technique, and was equipped with an automatic dilution system. In this study, the summation mode, which is a combination of LE and LS, was applied. Duplicate measurements were made for each sample at the appropriate time point using the following conditions: data collecting time, 60 s; flow rate, 60 mL/min; injection loop volume, 1.04 mL; syringe volume, 2.5 mL; second dilution factor, 40.

Sample Preparation for Assay A 100 μL aliquot of each blood sample was transferred to a microtube. A 200 μL aliquot of internal standard (IS) solution (8.3 ng/mL of CsD in methanol–0.3 mol/L $ZnSO_4$, 7 : 3 v/v) was added to each tube. Tubes were tapped and vortexed for a few minutes until the pellet was completely dispersed. After centrifugation at 12000 rpm for 5 min, the supernatant was filtered by a centrifugal filter device (Ultrafree-MC, 0.22 μm polyvinylidene difluoride (PVDF); Millipore, Billerica, MA, U.S.A.). After further centrifugation at 10000 rpm for 2 min, the filtered sample was directly applied to the liquid chromatography/mass spectrometry (LC/MS) system.

Due to difficulty in obtaining reference standards of CsA metabolites, the *in vitro* metabolic reaction was performed by following the method for rat liver microsomes, and reactants containing metabolized CsA were used to confirm the LC separation of CsA and its metabolites. First, a reduced nicotinamide adenine dinucleotide phosphate (NADPH) regenerating system (NRS; 1.7 mg/mL NADP, 7.8 mg/mL G-6-P, 6.0 units/mL G-6-PDH in 2% (w/v) $NaHCO_3$) was prepared. A 50 μL aliquot of rat liver microsomes, 5 μL of 500 ng/mL CsA in acetonitrile, and 320 μL of 50 mM Tris buffer were mixed in a microtube, and then pre-incubated at 37°C for 5 min. Next, 125 μL NRS was added and the solution was thoroughly mixed. After incubation at 37°C for 60 min, 500 μL internal standard solution was added to terminate the reaction. After centrifugation at 10000 rpm for 5 min, the supernatant was filtered, as described above, and applied to the LC/MS system.

Assay for Cyclosporine A and Its Metabolites CsA and its metabolites in whole blood were measured by LC/MS

system in accordance with Koseki *et al.*,[20] with some modifications. LC/MS was performed on a Shimadzu LCMS-2010 system that includes a constant pump, column thermostat, degasser, autosampler, and quadrupole mass spectrometer (Shimazdu Corporation, Kyoto, Japan). The HPLC column was a Symmetry C8 (4.6×75 mm, 3.5 μm; Waters, Milford, MA, U.S.A.) with a guard column (Opti-Guard-min C8, 1×15 mm; Optimize Technologies, Oregon City, OR, U.S.A.). LC/MS grade water and methanol were prepared as mobile phase A and B, respectively. The flow rate was set to 0.3 mL/min and the column temperature was 80°C. A linear gradient separation was used, with 72% of mobile phase B from 0 to 1 min, then 72% to 85% of mobile phase B over 5 min, holding for 3 min, and finally 72% of mobile phase B over 6 min. The total run time was 15 min for each injection. A 20 μL aliquot of each prepared sample was injected.

The mass spectrometer was interfaced with an electrospray ionization (ESI) source used in the positive ion mode. The following parameters were retained for optimal detection of all analytes: nitrogen gas flow rate, 1.5 L/min; interface voltage, 4.5 kV; desolvation line voltage and temperature, 20.0 V and 250°C, respectively; block heater, 200°C. For the determination of CsA and its metabolites as well as CsD, the sodium adducts were measured at *m/z* 1210.9 (AM4N), *m/z* 1224.9 (CsA), *m/z* 1238.9 (CsD, IS), and *m/z* 1240.9 (AM1, AM9, AM1c) by using selected ion monitoring (SIM). Retention times for AM1, AM9, AM1c, AM4N, CsA, and CsD were 8.6, 8.9, 9.5, 10.4, 11.4, and 12.2 min, respectively. Quantification of CsA and its metabolites was achieved with a calibration curve of CsA (concentration range, 7.8–500 ng/mL). The limit of detection (signal-to-noise ratio, 3) and quantification (signal-to-noise ratio, 10) of CsA was approximately 1.5 ng/mL and 5 ng/mL, respectively.

Animal Study The animal experiments were outsourced to Charles River Japan and performed in accordance with the Guideline for Animal Experiments of Charles River Japan. Male Sprague-Dawley rats weighing 220–250 g were fasted overnight with free access to water. The content of each CsA capsule product was diluted in distilled water to obtain a CsA concentration of 1.0 mg/mL. The CsA solution equivalent of 3.5 mg/kg CsA was orally administered to rats using a stomach sonde. Next, blood samples (300 μL) were collected from the jugular vein at 0.5, 1, 2, 3, 6, 12, and 24 h using a syringe flushed with 100 mg/mL ethylenediaminetetraacetic acid (EDTA), and stored at −80°C until analysis by LC/MS. The pharmacokinetic parameters of CsA and its metabolites, such as *AUC*, C_{max}, and time to reach C_{max} (T_{max}), were estimated by non-compartmental analysis using WinNonlin (version 5.2; Pharsight Corporation, Sunnyvale, CA, U.S.A.). The data between different products were compared for statistical significance by a Kruskal–Wallis test.

Results

Physicochemical Characteristics Neoral, a microemulsion pre-concentrate formulation, is composed of lipophilic solvent, hydrophilic solvent, surfactant, and drug. Table 1 shows the difference in additive composition of CsA capsule contents among products. First, we removed the contents of each capsule and compared the physical appearances before dispersion. Product A was the oil-based formulation Sandimmune, Product B was the innovator Neoral, and Products C to F were generic formulations. As seen in Fig. 1a, Product A and Product F were yellow, Product B and Product E were slightly yellow, and Product C and Product D were almost clear. Next, we dispersed the contents of 1 capsule in 10 mL of each test medium and compared the physical appearances (Fig. 1b). For the test media, water, 1st and 2nd Fluids for the dissolution test, artificial intestinal juice, Fasted State Simulated Intestinal Fluid (FaSSIF), and Fed State Simulated Intestinal Fluid (FeSSIF) were used. For all capsules the contents were homogeneously dispersed in each test medium except for Product A. The dispersion liquid of SEDDS is typically turbid and inhomogeneous, whereas that of SMEDDS is usually nearly clear. Thus, the dispersion state of the generics was obviously different from that of Product A (SEDDS). When the capsule contents were dispersed in water, Product B and Product E produced a clear and almost clear solution, respectively; Product F produced a white solution; and Product C and D produced bluish milky solutions. Assessment using the other test media indicated the same tendency. On the other hand, when the capsule contents were dispersed in FeSSIF, all generic products produced a white cloudy solution, whereas Product A produced a clear solution.

To quantify the degree of turbidity, we measured the absorbance at 600 nm of the dispersion solutions. The absorbance of the solutions formed by dispersion in water was high and showed the following order: B≈E<C=D<F<<<A. This same tendency was observed for the other test media (Fig. 2). These results correlated with the physical appearance of the solutions, including the significantly higher absorbance of generics dispersed in FeSSIF. In the case of Product F, a slight precipitate was formed in the dispersion solution several hours after initial dispersion (data not shown). The absorbance of Products B through E in each test medium decreased with increasing dilution, and no creaming or precipitation was observed. The solubility of dispersion solution was measured and found that there were no differences between the innovator and the generics with regard to solubility.

The distribution and number of particles of the microemulsion (or emulsion) in the dispersion solution were determined. The contents of 1 capsule were dispersed in 10 mL of water, and the distribution and number of particles (>0.5 μm) were measured by the single-particle optical sizing (SPOS) method. As seen in Fig. 3a, the particle size of the oil-based formulation Product A was significantly larger than that of the other products. Whereas the particle number (>0.5 μm) of products B and E was almost the same, that of Products C and D was 5-fold larger, and that of Product F was 25-fold larger, than that of Product B, which correlates with their physicochemical appearances (Fig. 3b). These results indicated that the particle distribution of generic products in solution is wider than that of the innovator.

The mean diameter and distribution of the particles of the microemulsion (or emulsion) in the dispersion solution formed from the capsule contents were measured by dynamic light scattering (DLS) (Fig. 4, Table 2). The mean diameter of each product in water at a 5-fold dilution was as follows: Product B, 26.4 nm; E, 29.7 nm; C, 74.8 nm; D, 64.5 nm; and F, 79.2 nm. Thus, the mean diameter of the generics tended to be larger than that of the innovator. The same tendency was observed in 1st and 2nd Fluids for the dissolution test, and FaSSIF. When the capsule contents of the generics were dispersed

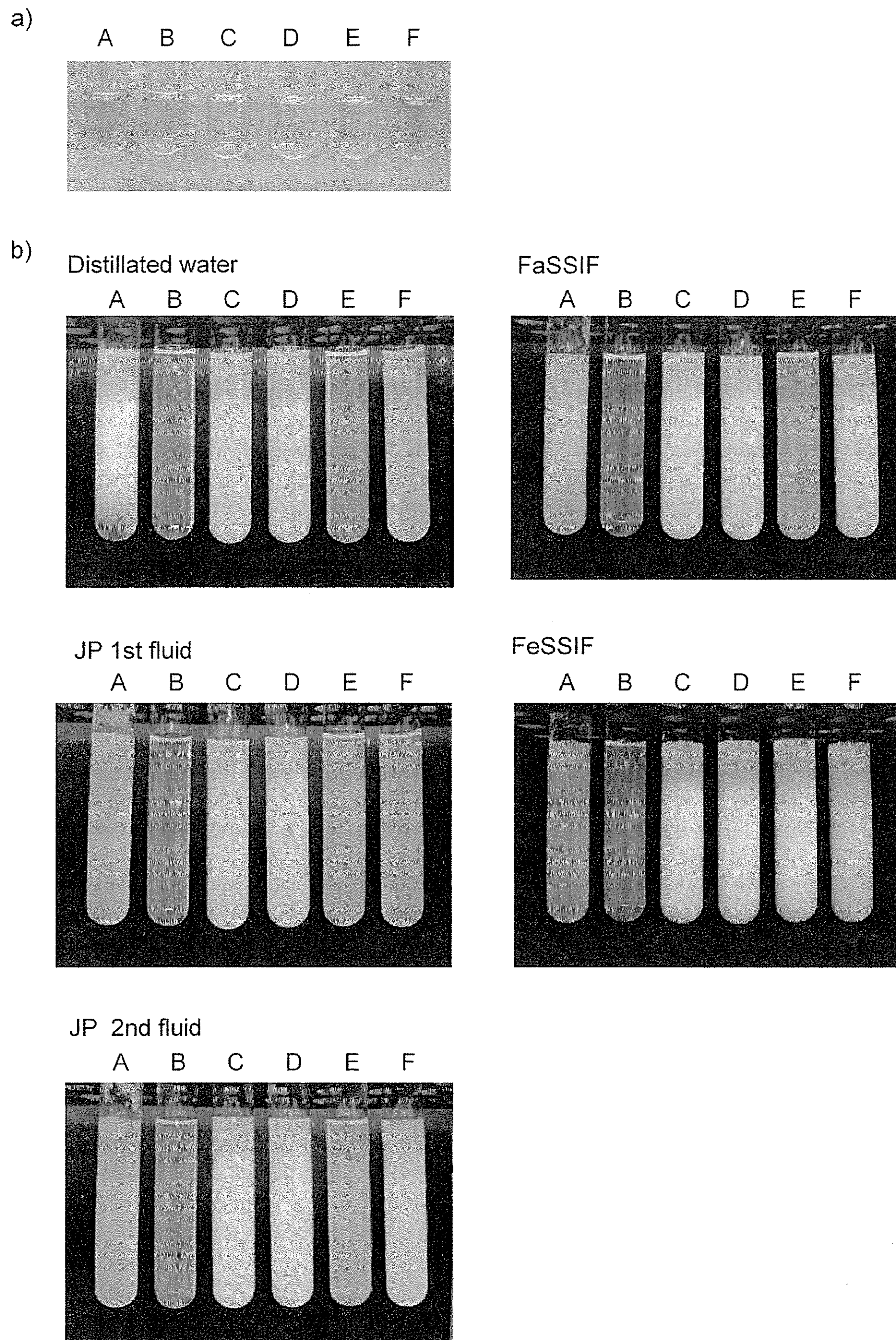

Fig. 1. Physical Appearances of (a) the Contents of Each CsA Capsule and (b) the Solution of the Contents of 1 CsA Capsule in 10 mL Water, 1st Fluid, 2nd Fluid, FaSSIF, and FeSSIF

in FeSSIF, the mean diameter of the generics increased to 100–200 nm. Among the generic products, dispersion of Product F in either the 2nd fluid or FaSSIF increased the mean diameter to 120–200 nm (Table 2), and the particle distribution expanded with increasing dilution (Fig. 4). In addition, when Product F was dispersed in either water or the 1st Fluid, the value of the mean diameter varied widely when compared with those of the other products (Table 2). These results, including those seen in Fig. 3, indicated that the particles in the dispersion solution of Product F could not be homogeneous. On the other hand, the mean diameter of the innovator, Product B, was very small (about 30 nm) in water, and in both 1st and 2nd test Fluids, and there were no changes in the mean diameter or distribution even when its capsule contents were dispersed in either FaSSIF or FeSSIF containing lecithin and taurocholic acid. This indicated that, after oral administration, a microemulsion of Product B is likely to be formed in the gastrointestinal tract. The mean particle diameter and distribution were not determined in the 1-fold and 5-fold dilutions of Product A because of the high scattering intensity. The small mean diameter of the generics in FeSSIF may be caused by multiple scattering.

Table 1. Composition of CsA Capsule Contents

	Product A	Product B	Product C	Product D	Product E	Product F
Solvent	Esterified corn oil	Glycerol esters of fatty acids	Propylene glycol esters of fatty acids	Propylene glycol esters of fatty acids	Propylene glycol esters of fatty acids	Propylene glycol esters of fatty acids
	Ethanol	Propylene glycol			Triethyl citrate	
	Corn oil	Ethanol			Sorbitan monolaurate	Ethanol
Surfactant		Polyoxyethylene hydrogenated castor oil	Polyoxyl 35 castor oil	Polyoxyl 35 castor oil	Polyoxyl 35 castor oil	Polyoxyl 35 castor oil
Other		Tocopherol	Other two components	Other two components		Other five components

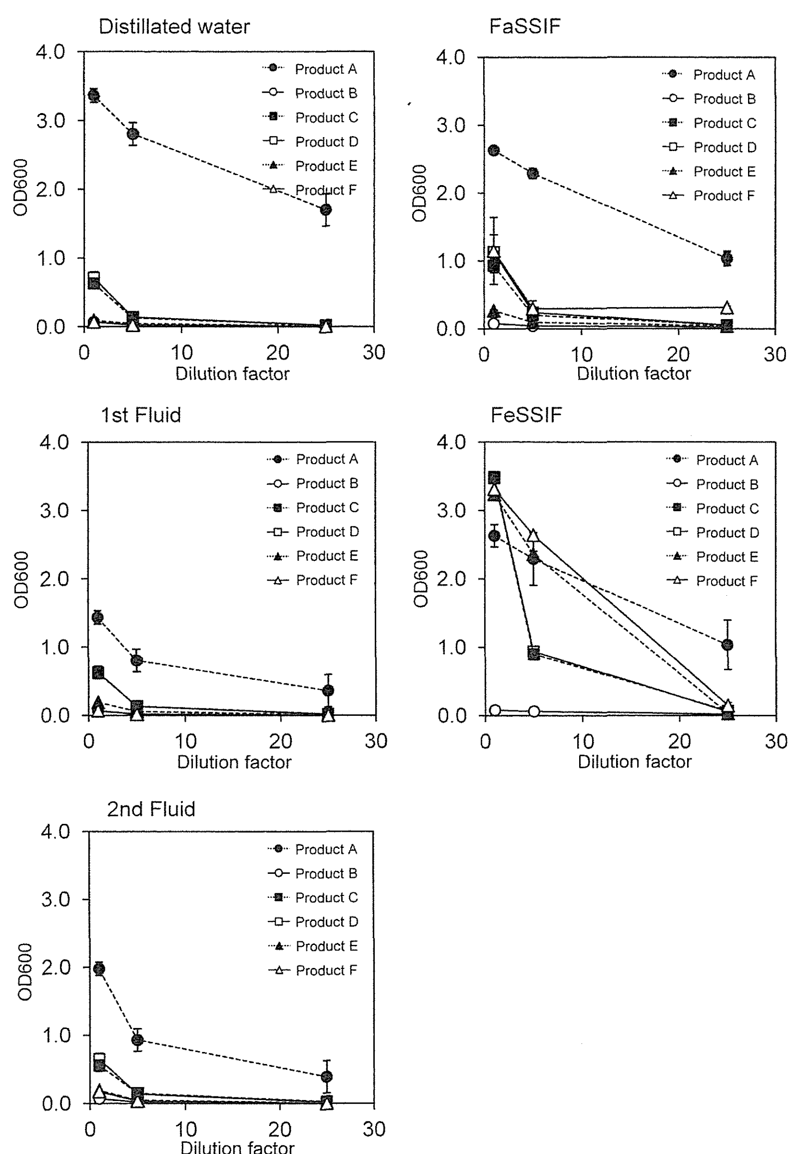

Fig. 2. Absorbance (600 nm) of the Suspension of the Contents of 1 CsA Capsule in 10 mL of Test Media and Diluted Solutions Thereof
Data are represented as the mean±S.D.

Pharmacokinetics of CsA and Its Metabolites in Rats The results described above demonstrate that, although all generic products were dispersed in each test medium unlike Product A, the physical appearance and particle diameter of the generic dispersion solutions were different from those of the innovator Product B. Therefore, we next assessed the blood concentration profiles of CsA and its metabolites (AM1, AM9, AM1c, and AM4N) after oral administration in rats (Fig. 5). The blood concentration was measured by liquid chromatography-mass spectrometry (LC-MS) analysis, and the